

SCATTERING STATES FROM
TIME-DEPENDENT DENSITY
FUNCTIONAL THEORY

BY ADAM WASSERMAN

A dissertation submitted to the
Graduate School—New Brunswick
Rutgers, The State University of New Jersey
in partial fulfillment of the requirements

for the degree of

Doctor of Philosophy

Graduate Program in Chemistry

Written under the direction of

Prof. Kieron Burke

and approved by

New Brunswick, New Jersey

October, 2005

ABSTRACT OF THE DISSERTATION

Scattering states from Time-dependent Density Functional Theory

by Adam Wasserman

Dissertation Director: Prof. Kieron Burke

Linear response time-dependent density functional theory is used to study low-energy elastic electron scattering from targets that can bind an extra electron. Exact formulas to extract scattering amplitudes from the susceptibility are derived in one dimension. A single-pole approximation for scattering phase shifts in three dimensions is derived, and shown to be more accurate than static exchange for singlet electron-He⁺ scattering. A novel formula to obtain elastic scattering t -matrix elements is derived for systems with spherical symmetry.

It is also shown that despite the incorrect asymptotic behavior of its potential, the time-dependent local density approximation can yield accurate optical spectra. The oscillator strengths of Rydberg excitations appear in the calculated spectrum as continuum contributions with excellent optical intensity. We explain why, illustrate this for the neon and helium atoms, and also discuss when such calculations of the optical response will be inaccurate. Finally, we show how the local density approximation yields accurate Rydberg excitation energies.

Acknowledgements

Thank you for everything, Kieron. And thank you for everything, Morrel, Neepa, and all group members, past and present. A picture collage with proper acknowledgements is available upon request.

Dedication

I often dream about interacting electrons. Sometimes it starts as a nightmare: I am sitting in the middle of an empty room, and there are hundreds of electrons flying around. The room is small (the spectrum is discrete). I have a pencil, and I'm scribbling some equations on a piece of paper, trying to describe what's going on. It's upsetting that my own presence there complicates matters further, since electrons are scattering off me in a random way. The interaction between electrons, and my own existence, makes this a hopeless task. I start hearing voices: "hopeless, hopeless..." (actually, I still dream in Spanish: "No hay esperanza, ninguna esperanza..."). But it is then, when I am at the edge of despair, that the electrons suddenly stop moving. The walls of the room start changing shape, curving as in a Van Gogh painting, and when this magic transformation is over, electrons start moving again, but in a much simpler way: they still bounce from me and the distorted walls, but they don't seem to be interacting among themselves anymore! I look at the piece of paper in my hands, cross out the equations I was trying to solve before, and in ecstasy write down a much simpler set of equations for non-interacting electrons. The nightmare gives way to a sweet dream. In happiness, I stare at the new equations, smiling, and the voices start singing: "DFT, DFT..."

Chapter 3 is dedicated to the Local Density Approximation on the occasion of its 40th birthday.

Table of Contents

Abstract	ii
Acknowledgements	iii
Dedication	iv
List of Tables	viii
List of Figures	ix
1. Introduction	1
1.1. Electron-molecule scattering	2
1.1.1. Wavefunction methods	3
1.1.2. Density functional methods	5
Elementary example	5
1.2. Time-dependent Density Functional Theory (linear response)	6
2. Scattering amplitudes from Time-dependent Density Functional Theory	9
2.1. Preliminaries	9
2.2. One dimension	11
2.2.1. Transmission amplitudes from the susceptibility	11
Illustration of Eq.(2.12)	14
2.2.2. TDDFT equation for transmission amplitudes	15
2.2.3. An example, $N = 0$, trivial.	16
2.2.4. Another example, $N = 1$, not trivial.	17

2.3.	Three dimensions	20
2.3.1.	Single Pole Approximation in the continuum	20
2.3.2.	Partial-wave analysis of scattering within TDDFT	23
	Linear response equation at large distances	24
	Asymptotic behavior of Green functions	25
	TDDFT equation for t -matrix elements and phase shifts	27
2.4.	Summary and outlook	28
3.	Accurate Rydberg excitations from the Local Density Approximation	30
3.1.	Rydberg oscillator strengths from LDA scattering states	33
3.1.1.	Truncated and shifted Coulomb potential	33
3.1.2.	LDA potentials	34
3.2.	Rydberg excitation energies from LDA scattering states	41
3.2.1.	Quantum defect from its orbital	43
3.2.2.	Two examples	43
3.2.3.	Results for Helium and Neon	46
Appendix A.	Extracting transmission amplitudes from the susceptibility in 1d	52
A.1.	Derivation of Eq.(2.11)	52
A.2.	Derivation of Eq.(2.12)	53
Appendix B.	Elastic scattering in 1d	55
B.1.	Parity-wave analysis of 1d-scattering	55
B.2.	Phase shifts	56
B.2.1.	Particular cases	56
B.3.	Transmission amplitude from Lippmann-Schwinger's equation	57
B.4.	Born approximation in TDDFT	57

Appendix C. One electron: Susceptibility from the Green function.	59
Appendix D. Hartree-exchange kernel for two contact-interacting electrons	61
Appendix E. Numerical calculation of bound→free TDDFT matrix elements	63
E.1. Hartree-exchange	63
E.2. Correlation	64
E.3. Note about the hybrid kernel employed	65
Appendix F. High frequency behavior of optical response	66
F.1. $p \rightarrow s$ transitions	66
F.2. $s \rightarrow p$ transitions	67
References	67
References	68
Curriculum Vitae	75

List of Tables

3.1. Oscillator strengths for the first six discrete $2p \rightarrow ns$ transitions in Ne.[LDA numbers extracted from the height of the LDA continuum curve at the exact transition frequencies].	36
3.2. Transition frequencies and oscillator strengths in atomic units for the first six discrete $2p \rightarrow ns$ transitions in Ne, from the exact and LDA KS potentials.	49

List of Figures

2.1. Cartoon of Eq.(2.11). To extract the transmission amplitude for an electron of energy ε scattering from an N -electron target: apply a perturbation of frequency $\varepsilon + I$ on the far left of the $(N + 1)$ -ground-state system (I is its first ionization energy), and look at how the density changes oscillate on the far right. Once amplified, the amplitude of these oscillations correspond to $t(\varepsilon)$	13
2.2. Transmission coefficient $T_s = t_s ^2$ for an electron scattering from the 1d-potential $v_s(x) = -Z_1\delta(x) - Z_2\delta(x - a)$. $Z_1 = Z_2 = 1$ in this plot, and $a = 1$ as well. Interesting: perfect transmission at $k = 0$ due to proximity of the two delta-function wells.	15
2.3. Left: cartoon of an electron scattering from a negative delta-function potential. Right: cartoon of an electron bound to the same potential; the ground-state density decays exponentially, just as in hydrogenic ions in 3d.	16
2.4. Left: cartoon of an electron scattering from 1d-He ⁺ . Right: cartoon of two electrons bound to the delta function in a singlet state.	17
2.5. Real and imaginary parts of the KS transmission amplitude t_s , and of the interacting singlet and triplet amplitudes, for the model system of Eq.(2.21). $Z = 2$ and $\lambda=0.5$ in this plot.	19

2.6.	s -phase shifts as a function of energy for electron scattering from He^+ . <i>Dashed lines</i> : the line labeled KS corresponds to the phase shifts from the <i>exact</i> KS potential of the He atom; the other dashed lines correspond to the TDDFT singlet and triplet phase shifts calculated in the present work according to Eq.(2.37). <i>Solid lines</i> : accurate wavefunction calculations of electron- He^+ scattering from Ref.[50]. The solid line in the center is the average of singlet and triplet phase shifts. <i>Dotted lines</i> : Static exchange calculations, from Ref.[51]. The asterisks at zero energy correspond to extrapolating the bound \rightarrow bound results of Ref.[49].	22
3.1.	Oscillator strengths (in inverse Hartrees) for the $2p \rightarrow ns$ transitions in Ne as a function of photon energy (in Hartrees), from the exact KS potential, and from the LDA one. The discrete spectrum has been multiplied by the density-of-states factor (see text). . . .	32
3.2.	Oscillator strengths (in inverse Hartrees) corresponding to $1s \rightarrow np$ transitions (only shown for $n \geq 4$) for a pure Coulomb and the truncated-Coulomb potential given by Eq. (3.3) with $1/C = 20$. . .	34
3.3.	Ne atom: the top curve shows the difference between the LDA and exact XC-potential. The bottom curves show v_s^{exact} and v_s^{LDA} . In the valence region (shaded) the two potentials run almost parallel.	35
3.4.	Bottom panel: Integrated oscillator strength as a function of frequency for the pure and truncated coulomb potentials; $r_0 = 20$ in this plot.	37
3.5.	Bottom panel: Integrated oscillator strength as a function of frequency for the exact and LDA potential of the Ne atom	37
3.6.	Ne atom: LDA <i>continuum</i> state at energy $E=0.2853$, and exact energy-normalized $8s$ <i>bound</i> orbital, along with the LDA and exact $2p$ orbitals.	38

3.7. The threshold of the truncated spectrum passes through the $1s \rightarrow 3p$ discrete transition of the pure Coulomb potential as r_0 goes from 18 to 16. 39

3.8. $2p \rightarrow nd$ spectrum of Ne, plotted as in Fig. 1. as a function of photon energy, from the exact KS potential, and from the LDA one. 40

3.9. He atom: The top panel shows the bare exact KS and LDA spectra, and the lower panel shows the TDDFT corrected spectra, LDA/ALDA results are from [72] but unshifted; the exact calculations are from [73], multiplied by the density of states factor (see text), and the experimental results are from [74]. 40

3.10. *Left:* Potential with constant core ($C = 1$) and Coulomb tail beginning at $r_0 = 1$. Its energy spectrum is indicated by horizontal lines. *Right:* s -quantum defect as a function of n for the potential of the first example. The quantum defect is a smooth function of n and converges rapidly to its asymptotic value, $\mu = -0.441$ 45

3.11. Solution of Eq.(3.9) for μ as a function of r , for the potential of the first example; the logarithmic derivative of the $n = 20$ orbital was found numerically as a function of r , and at each location r , it was inserted into Eq.(3.9) to get $\mu(r)$ 45

3.12. Comparison of the exact KS potential of the He atom [48] (solid line), and the LDA potential (dashed line). The Coulomb potential is also shown (dotted line). At $r \sim 1$ the exact potential is almost Coulombic. The inset shows the potentials themselves. 46

3.13. s -quantum defect as a function of n for the exact KS potential [48] of the He atom. The quantum defect converges rapidly to its asymptotic value, $\mu = 0.213$ 47

3.14. He atom: solution of Eq.(3.9) for μ as a function of r ; The $n = 20$ orbital was used 48

3.15. Radial orbitals of He: LDA orbital of energy $E=0.333$ and exact 20s orbital; the HOMO is also shown. Notice that the LDA scattering orbital and the exact KS Rydberg orbital are very close in the region $1 < r < 2$, where the quantum defect can be extracted (see text, and Fig.3.16). The fact that the LDA orbital has an incorrect asymptotic behavior at large r is irrelevant for the value of μ , as well as for optical absorption [77]	48
3.16. He atom: solution of Eq.(3.9) for μ as a function of r ; The $n = 20$ orbital was used for the exact case, and the $E=0.333$ orbital was used for the LDA (the value of n in Eq.(3.9) was set large enough in this case to ensure convergence)	49
3.17. Ne atom: solution of Eq.(3.9) for μ as a function of r ; The $n = 8$ orbital was used for the exact case, and the $E=0.285$ orbital was used for the LDA.	50
3.18. Ne atom: Like in Fig.(3.1), but now using the LDA excitation energies as listed in Table 3.2.	50
C.1. Although $\chi_s(x, -x; \varepsilon)$ decays exponentially (because the density decays exponentially), it oscillates at large distances, and the amplitude of these oscillations yields the transmission coefficient. $Z = 1$ in this plot.	60

Chapter 1

Introduction

This thesis is being defended in 2005, the “World Year of Physics”. With the 100th anniversary of Einstein’s *annus mirabilis*, there have been many interesting discussions about what makes some lines of research more *fundamental* than others [1]. Though not as widespread as it used to be, the opinion that the *only* truly fundamental research is the one directed to discover the “ultimate” laws of nature (in high energy physics and cosmology) is still prevalent in some circles. But equally fundamental research is required at each level of complexity, because “*more is different*” [2]. The same status of “fundamental research” is shared by a third type of research, which is neither directed to find the ultimate laws of nature, nor to describe emergent new phenomena. Its aim is to study well-understood phenomena, but from new and different perspectives. Just as artists stepping aside from an almost-finished painting to see it from a different angle, practitioners of this third type of research step aside to see a theory from different angles, gaining new insights that will allow them to solve problems that could not be solved otherwise. The artist can always go back to the painting and retouch it. A good example is the research that led to the formulation of Density Functional Theory (DFT) [3]. Walter Kohn stepped aside to look at the well-established quantum theory of matter, from a different angle. Some aspects of the theory started to look much more transparent from the new perspective. In order to share his vision with the rest of us, he proposed (with Lu Sham) a practical method to calculate ground-state properties of many-electron systems [4]. The method was so efficient, accurate, and easy to implement that the applications of

DFT have seen an exponential growth since then, first in solid-state physics, and then – when more sophisticated functionals were developed – in quantum chemistry. At the time it was formulated, however, DFT did not come as a solution to any “fundamental” problem in physics or chemistry (type III research), yet it opened-up new roads that have greatly contributed to the advancement of science [5]. I will not review here the theory of ground-state DFT [6]-[9].

The field of low-energy electron-molecule scattering faces difficulties which are similar in nature to those faced by quantum chemistry before the advent of DFT. Nothing is fundamentally unclear about it, since the equations that ought to be solved are well-known and can be written down. The problem is that for most cases of interest they cannot be *solved* with the desired accuracy.

1.1 Electron-molecule scattering

Electrons are constantly colliding with atoms and molecules: in chemical reactions, in our atmosphere, in stars, plasmas, in a molecular wire carrying a current, or when the tip of a scanning tunneling microscope injects electrons to probe a surface. When the collision occurs at low energies, the calculations become especially difficult due to correlation effects between the projectile electron and those of the target. These *bound-free* correlations are very important. For example, it is due to bound-free correlations that ultra-slow electrons can break up RNA molecules [10] causing serious genotoxic damage. The accurate description of correlation effects when the targets are so complex is a major challenge. Existing approaches based on wavefunction methods, developed from the birth of quantum mechanics and perfected since then to reach great sophistication [11], cannot overcome the exponential barrier resulting from solving the many-body Schrödinger equation when the number of electrons in the target is large. Wavefunction-based methods can still provide invaluable insights in such complex cases, provided powerful

computers and smart tricks are employed (see e.g.[12] for low-energy electron scattering from Uracil), but a truly ab-initio approach circumventing the exponential barrier would be most welcome. The purpose of Chapter 2 is to describe several results relevant to this goal.

1.1.1 Wavefunction methods

When an electron with momentum \mathbf{k}_i collides with an N -electron atom which is initially in state ψ_i^{target} , the differential scattering cross section for a transition to a final state $(\mathbf{k}_j, \psi_j^{target})$ is given by [13] (we will always use atomic units in this work):

$$\frac{d\sigma_{ji}}{d\Omega} = \frac{k_j}{k_i} |f_{ji}(\theta, \phi)|^2, \quad (1.1)$$

where the scattering amplitudes $f_{ji}(\theta, \phi)$ determine the asymptotic form of the spatial $(N + 1)$ -electron wavefunction:

$$\Psi_i \xrightarrow{r \rightarrow \infty} \psi_i^{target} e^{ik_i z} + \sum_j \psi_j^{target} f_{ji}(\theta, \phi) \frac{e^{ik_j r}}{r}, \quad (1.2)$$

which is an eigenstate of the $(N + 1)$ -electron Hamiltonian:

$$\hat{H}_{N+1} \Psi_i = E_i \Psi_i \quad (1.3)$$

$$\hat{H}_{N+1} = \sum_{i=1}^{N+1} \left(-\frac{1}{2} \nabla_i^2 - \frac{Z}{r_i} \right) + \sum_{i>j=1}^{N+1} \frac{1}{r_{ij}} \quad (1.4)$$

To get the exact f_{ji} 's we would need to find the exact Ψ_i 's, which would imply the hopeless task of solving Eq.(1.3) exactly. Most approximation methods start from the following expansion of Ψ_i :

$$\Psi_i = \hat{A} \sum_j \tilde{\psi}_j^{target}(\mathbf{x}_1 \dots \mathbf{x}_N; \hat{r}_{N+1} \sigma_{N+1}) \frac{1}{r_{N+1}} F_{ji}(\mathbf{r}_{N+1}) + \sum_j \chi_j(\mathbf{x}_1 \dots \mathbf{x}_{N+1}) a_{ji} \quad (1.5)$$

where \mathbf{x}_i stands for $\{\mathbf{r}_i, \sigma_i\}$, and the channel functions $\tilde{\psi}_j^{target}$ are obtained by coupling the target states ψ_j^{target} with the spin-angle functions of the scattered electron to form eigenstates of the total orbital and spin angular momentum operators (and the parity operator). The F_{ji} are radial functions describing the

motion of the scattered electron, and the operator \hat{A} antisymmetrizes the first summation with respect to interchange of any pair of electrons. If the second sum in Eq.(1.5) is omitted, the equation is referred to as the *close coupling* expansion, but inclusion of this term allows for a better treatment of correlation effects; the χ_j are square integrable correlation functions. Substituting Eq.(1.5) into Eq.(1.3), projecting onto the channel functions $\tilde{\psi}_j^{target}$ and χ_j , and eliminating the coefficients a_{ji} of the resulting equations, one gets a set of coupled integrodifferential equations for the F_{ji} :

$$\left(\frac{d^2}{dr^2} - \frac{l_j(l_j + 1)}{r^2} + \frac{2Z}{r} + k_j^2 \right) F_{ji}(r) = 2 \sum_k (V_{jk} + W_{jk} + X_{jk}) F_{ki}(r) \quad , \quad (1.6)$$

where l_j is the orbital angular momentum of the scattered electron and V_{jk} , W_{jk} , and X_{jk} are the partial wave decompositions of the Hartree, exchange and correlation potentials. Once Eqs.(1.6) are solved, the scattering amplitudes can be determined from the asymptotic behavior of the F_{ji} . There are several families of computational methods to solve Eqs.(1.6). Two of the most popular ones are the *R*-matrix method [14] and variational methods [15]. In the *R*-matrix method one solves the problem of the $(N + 1)$ -electron system in a region close to the target, and matches later these “inner solutions” with “outer solutions” that obey appropriate boundary conditions; the *R*-matrix is a mathematical device for doing this matching procedure. In the variational methods, parameters in the wave function are determined so that a variational functional is made stationary.

Very accurate scattering cross-sections have been obtained using these methods for low-energy electron scattering off light atoms [16], and the current generation of massively parallel computers has allowed the calculation of accurate cross sections for electrons scattering off heavier ions, like Ni(IV) [17]. But the computational cost of wave-function methods grows exponentially with the number of electrons (at best like N^4), so only through approximations especially crafted to describe a particular system can they be successfully applied to obtain accurate scattering information in these complex cases. An example of this is the case of

electron – CO₂ scattering [18]. The low energy integrated cross sections for this process have two distinctive features: a rise in the cross sections below 2.0eV and a resonance peak centered near 3.8eV. Even though these features were observed experimentally many years ago [19] only recently was their detailed origin understood as a consequence of subtle bound-free correlation effects [20], absent from close-coupling calculation and hard to capture by any of the existing approximations.

1.1.2 Density functional methods

In accordance with the Hohenberg-Kohn theorem [3], the scattering cross sections defined before, Eq.(1.1), are functionals of the ground-state density of the $(N+1)$ -electron system: knowledge of the ground-state density of an $(N+1)$ -electron system is enough to determine, *in principle*, the results of the collision of one electron with the corresponding N -electron target. This has no meaning when the lowest energy state of the $(N+1)$ -electron system is unbound, so we will restrict our discussion to systems that bind $N+1$ electrons: positive ions, and most neutral targets.

Elementary example

Consider one electron in one dimension scattering off an $N = 0$ target in the presence of a negative delta function $V(x) = -Z\delta(x)$ of strength Z . This potential admits one bound state of energy $-Z^2/2$. The transmission coefficient must be singular at that energy, and should therefore be of the form $T(\varepsilon) = f(\varepsilon)/(\varepsilon + Z^2/2)$, where $f(\varepsilon)$ must go to zero as $\varepsilon \rightarrow 0$ and to ε as $\varepsilon \rightarrow \infty$. The simplest guess $f(\varepsilon) = \varepsilon$ provides in fact the exact answer: $T(\varepsilon) = \varepsilon/(\varepsilon + Z^2/2)$. Notice how easy it was to construct a transmission coefficient density functional in this

case:

$$T[\rho](\varepsilon) = \frac{\varepsilon}{\varepsilon - E_0[\rho]} \quad , \quad (1.7)$$

where ρ is the ground state density of the $(N+1)$ -electron system, and $E_0[\rho]$ is the exact ground-state energy functional. Since the functional $T[\rho]$ is exact for this system, we can think of it as a limiting case of the unknown universal transmission functional in one dimension, and expect it to be a good approximation for other systems with only one bound state.

This could be a good way of approaching the general problem of electron-molecule scattering from a density-functional perspective if accurate excited-state energy functionals were available. But although much progress has been achieved developing better and better approximations to the ground-state energy functional [4, 21, 22, 23], developing functionals of the ground-state density for excited state properties has proven to be a tortuous path [24, 25]. A more direct approach to excited states relies on time-dependent DFT (TDDFT). The theory is based on the Runge-Gross theorem [26], which establishes a one to one mapping between time-dependent densities and time-dependent external potentials, under certain conditions that will not be reviewed here (this is discussed in, e.g., refs.[27] and [28]).

1.2 Time-dependent Density Functional Theory (linear response)

TDDFT applies to any electronic system subject to any (strong or weak) time-dependent potential [29], but we will be concerned here only about the *linear response regime* [30, 31], which we outline now.

Imagine that a small time-dependent perturbation $\delta v_{\text{ext}}(\mathbf{r}', t')$ is applied to a system of interacting electrons in its ground-state. Then the density will change

by an amount $\delta\rho(\mathbf{r}, t)$ determined by the susceptibility:

$$\chi(\mathbf{r}, t, \mathbf{r}', t') = \left. \frac{\delta\rho(\mathbf{r}, t)}{\delta v_{\text{ext}}(\mathbf{r}', t')} \right|_{\rho} \quad (1.8)$$

where ρ is the ground-state density. A system of *non-interacting* electrons with the same ρ has a different susceptibility, and a different perturbation $\delta v_s(\mathbf{r}', t')$ is needed in order to produce the same density change $\delta\rho(\mathbf{r}, t)$. The Kohn-Sham susceptibility is given by:

$$\chi_s(\mathbf{r}, t, \mathbf{r}', t') = \left. \frac{\delta\rho(\mathbf{r}, t)}{\delta v_s(\mathbf{r}', t')} \right|_{\rho} \quad (1.9)$$

The two, χ and χ_s are therefore related by:

$$\chi(\mathbf{r}, t, \mathbf{r}', t') = \int d\mathbf{x} \int d\tau \left. \frac{\delta v_s(\mathbf{x}, \tau)}{\delta v_{\text{ext}}(\mathbf{r}', t')} \right|_{\rho} \chi_s(\mathbf{r}, t, \mathbf{x}, \tau) \quad (1.10)$$

The potential $v_s(\mathbf{r}, t)$ is uniquely determined by $v_{\text{ext}}(\mathbf{r}, t)$ [26] according to:

$$v_s(\mathbf{r}, t) = v_{\text{ext}}(\mathbf{r}, t) + \int d^3r' \frac{\rho(\mathbf{r}', t)}{|\mathbf{r} - \mathbf{r}'|} + v_{\text{xc}}(\mathbf{r}, t) \quad , \quad (1.11)$$

where $v_{\text{xc}}(\mathbf{r}, t)$ is the time-dependent exchange-correlation potential defined by the requirement that non-interacting electrons moving in the presence of $v_s(\mathbf{r}, t)$ have the same time-dependent density $\rho(\mathbf{r}, t)$ as that of the interacting system.

Taking the functional derivative of $v_s(\mathbf{r}, t)$ with respect to $v_{\text{ext}}(\mathbf{r}', t')$ and inserting it into Eq.(1.10) one gets the Dyson-like response equation:

$$\begin{aligned} \chi(\mathbf{r}, t, \mathbf{r}', t') &= \chi_s(\mathbf{r}, t, \mathbf{r}', t') + \int d\mathbf{x} \int d\tau \int d\mathbf{x}' \int d\tau' \chi_s(\mathbf{r}, t, \mathbf{x}, \tau) \\ &\times \left(\frac{\delta(\tau - \tau')}{|\mathbf{x} - \mathbf{x}'|} + f_{\text{xc}}[\rho](\mathbf{x}, \tau, \mathbf{x}', \tau') \right) \chi(\mathbf{x}', \tau', \mathbf{r}', t') \end{aligned} \quad (1.12)$$

where

$$f_{\text{xc}}[\rho](\mathbf{x}, \tau, \mathbf{x}', \tau') \equiv \left. \frac{\delta v_{\text{xc}}(\mathbf{r}, t)}{\delta \rho(\mathbf{r}', t')} \right|_{\rho} \quad (1.13)$$

is the time-dependent exchange-correlation kernel. Fourier transforming with respect to $(t - t')$, Eq.(1.12) becomes:

$$\chi(\mathbf{r}, \mathbf{r}'; \omega) = \chi_s(\mathbf{r}, \mathbf{r}'; \omega) + \int d\mathbf{x} \int d\mathbf{x}' \chi_s(\mathbf{r}, \mathbf{x}; \omega) f_{\text{Hxc}}[\rho](\mathbf{x}, \mathbf{x}'; \omega) \chi(\mathbf{x}', \mathbf{r}'; \omega) \quad (1.14)$$

This is the central equation of the linear response formalism of TDDFT, and will be the starting point for our developments of Chapter 2. We show there that an analysis of Eq.(1.14) when $|\mathbf{r}|$ and $|\mathbf{r}'|$ are very large, leads to alternative ways of obtaining scattering information.

Whereas in Chapter 2 we deal with the formalism of scattering within TDDFT, in chapter 3 we study the performance of the simplest approximation to the exchange-correlation potential, i.e., the local density approximation (LDA). We show that from the low-energy scattering states of an LDA potential one can obtain information about the true (bound) Rydberg states of the system under consideration.

Chapter 2

Scattering amplitudes from Time-dependent Density Functional Theory

2.1 Preliminaries

Consider a slow electron approaching an atom or molecule that has N electrons, and is assumed to be in its ground state, with energy E_0^N . The asymptotic kinetic energy of the incoming electron is ε , so the whole system of target plus electron has a total energy of $E_0^N + \varepsilon$. This is an excited state of the $(N + 1)$ -electron system, and as such, it can be described by the linear response formalism of TDDFT starting from the *ground state* of the $(N + 1)$ -electron system. We will explain how.

The targets we will consider must be able to bind an extra electron. For example, take the target to be a positive ion, so that the $(N + 1)$ -electron system, with ground-state energy E_0^{N+1} , is neutral. It is well known how to employ TDDFT to calculate, e.g., excitation energies corresponding to bound \rightarrow bound transitions from the ground state [32], but in the scattering situation considered here the excitation energy is known in advance: it is $I + \varepsilon$, where I is the first ionization energy of the $(N + 1)$ -system, $I = E_0^N - E_0^{N+1}$. It is the scattering *phase shifts*, rather than the energies, that are of interest in the scattering regime.

The TDDFT approach to scattering that we are about to discuss [33] is very different from wavefunction-based scattering methods (as outlined in Chapter 1), yet *exact* in the sense that if the ground-state exchange-correlation potential (v_{xc}) and time-dependent exchange-correlation kernel (f_{xc}) were known exactly,

we could then (in principle) calculate the *exact* scattering phase shifts for the system of $N + 1$ interacting electrons. Any given approximation to v_{XC} and f_{XC} leads in turn to definite predictions for the phase shifts. The method involves the following three steps: (1) Finding the ground-state Kohn-Sham potential of the $(N + 1)$ -electron system, $v_s^{N+1}(\mathbf{r})$, (2) Solving a *potential scattering* problem, namely, scattering from $v_s^{N+1}(\mathbf{r})$, and (3) Correcting the Kohn-Sham scattering phase shifts towards the true ones, via linear response TDDFT.

As stated in the Introduction, the central equation of the linear response formalism of TDDFT is the Dyson-like response equation relating the susceptibility $\chi^{N+1}(\mathbf{r}, \mathbf{r}'; \omega)$ of a system of interacting electrons with that of its ground-state Kohn-Sham analog, $\chi_s^{N+1}(\mathbf{r}, \mathbf{r}'; \omega)$ [31]. The $N + 1$ superscript was added in order to emphasize that we are going to perturb the ground-state of the $(N + 1)$ -electron system, where N is the number of electrons of the target. In what follows, however, for notational simplicity, the $(N + 1)$ superscript will be dropped from all quantities. In operator form (* indicates spatial and spin convolution):

$$\chi = \chi_s + \chi_s * f_{\text{HXC}} * \chi \quad , \quad (2.1)$$

where f_{HXC} is the Hartree-exchange-correlation kernel defined in Eq.(1.13):

$$f_{\text{HXC}}[\rho](\mathbf{r}, \mathbf{r}'; t - t') \equiv \frac{\delta(t - t')}{|\mathbf{r} - \mathbf{r}'|} + \left. \frac{\delta v_{\text{XC}}(\mathbf{r}, t)}{\delta \rho(\mathbf{r}', t')} \right|_{\rho} \quad , \quad (2.2)$$

a functional of the $(N + 1)$ -ground-state density $\rho(\mathbf{r})$. In Eq.(2.2), $v_{\text{XC}}(\mathbf{r}, t)$ is the time-dependent exchange-correlation potential induced when a time-dependent perturbation is applied to the $(N + 1)$ -ground state. We write the spin-decomposed susceptibility in the Lehman representation:

$$\chi_{\sigma\sigma'}(\mathbf{r}, \mathbf{r}'; \omega) = \left[\sum_n \frac{F_{n\sigma}(\mathbf{r}) F_{n\sigma'}^*(\mathbf{r}')}{\omega - \Omega_n + i0^+} + cc(\omega \rightarrow -\omega) \right] \quad , \quad (2.3)$$

with

$$F_{n\sigma}(\mathbf{r}) = \langle \Psi_0 | \hat{\rho}_{\sigma}(\mathbf{r}) | \Psi_n \rangle \quad ; \quad \hat{\rho}_{\sigma}(\mathbf{r}) = \sum_{i=1}^N \delta(\mathbf{r} - \hat{\mathbf{r}}_i) \delta_{\sigma\hat{\sigma}_i} \quad (2.4)$$

where Ψ_0 is the ground state of the $(N + 1)$ -electron system, Ψ_n its n^{th} excited state, and $\hat{\rho}_\sigma(\mathbf{r})$ is the σ -spin density operator. In Eq.(2.3), Ω_n is the $\Psi_0 \rightarrow \Psi_n$ transition frequency. The term “ $cc(\omega \rightarrow -\omega)$ ” stands for the complex conjugate of the first term with ω substituted by $-\omega$. The sum in Eq.(2.3) should be understood as a sum over the discrete spectrum and an integral over the continuum. *All* excited states (labeled by n) with non-zero $F_{n\sigma}(\mathbf{r})$ contribute to the susceptibility. In particular, the scattering state discussed before, consisting on a free electron of energy ε and an N -electron target, contributes too. How to extract from the susceptibility the scattering information about this single state?: the question will be answered in the following sections, starting in one dimension.

In Sec.2.2 we derive TDDFT equations for one-dimensional scattering, and work out in detail an example to show how to calculate transmission and reflection amplitudes in TDDFT. The discussion is then generalized in Sec.2.3 to three dimensions, where we explain how the familiar single pole approximation for bound \rightarrow bound transitions can be continued to describe bound \rightarrow continuum transitions to get information about scattering states, and how an analysis of Eq.(2.1) at large distances leads to a TDDFT equation for t -matrix elements. We end this Chapter in Sec.2.4 with a brief summary and outlook.

2.2 One dimension

2.2.1 Transmission amplitudes from the susceptibility

Consider large distances, where the $(N + 1)$ -electron ground-state density is dominated by the decay of the highest occupied Kohn-Sham orbital [34]; the ground-state wavefunction behaves as [35]:

$$\Psi_0 \underset{x \rightarrow \infty}{\sim} \psi_0^N(x_2, \dots, x_{N+1}) \sqrt{\frac{\rho(x)}{N + 1}} S_0(\sigma, \sigma_2, \dots, \sigma_{N+1}) \quad (2.5)$$

where ψ_0^N is the ground-state wavefunction of the target, S_0 the spin function of the ground state and $\rho(x)$ the $(N + 1)$ -electron ground-state density. Similarly, the asymptotic behavior of the n^{th} excited state is:

$$\Psi_n \xrightarrow{x \rightarrow \infty} \psi_{n_t}^N(x_2, \dots, x_{N+1}) \frac{\phi_{k_n}(x)}{\sqrt{N+1}} S_n(\sigma, \sigma_2, \dots, \sigma_{N+1}) \quad (2.6)$$

where $\psi_{n_t}^N$ is an eigenstate of the target (labeled by n_t), S_n is the spin function of the n^{th} excited state, and $\phi_{k_n}(x)$ a one-electron orbital.

The contribution to $F_{n\sigma}(x)$ (Eq.(2.4)) from channels where the target is excited vanishes as $x \rightarrow \infty$ due to orthogonality. We therefore focus on *elastic* scattering only. Inserting Eqs.(2.5) and (2.6) into the 1d-version of Eq.(2.4), and taking into account the antisymmetry of both Ψ_0 and Ψ_n ,

$$F_{n\sigma}(x) \xrightarrow{x \rightarrow \infty} \sqrt{\rho(x)} \phi_{k_n}(x) \delta_{0,n_t} \sum_{\sigma_2 \dots \sigma_{N+1}} S_0^*(\sigma \dots \sigma_{N+1}) S_n(\sigma \dots \sigma_{N+1}) \quad (2.7)$$

The susceptibility at large distances is then obtained by inserting Eq.(2.7) into the 1d-version of Eq.(2.3):

$$\chi(x, x'; \omega) = \sum_{\sigma\sigma'} \chi_{\sigma\sigma'}(x, x'; \omega) \xrightarrow{x, x' \rightarrow \pm\infty} \sqrt{\rho(x)\rho(x')} \sum_n \frac{\phi_{k_n}(x)\phi_{k_n}^*(x')}{\omega - \Omega_n + i\eta} \delta_{0,n_t} \delta_{S_0, S_n} + cc(\omega \rightarrow -\omega) \quad (2.8)$$

Since only scattering states of the $(N + 1)$ -electron optical potential contribute to the sum in Eq.(2.8) at large distances, it becomes an integral over wavenumbers $k = \sqrt{2\varepsilon}$, where ε is the energy of the projectile electron:

$$\sum_n \frac{\phi_{k_n}(x)\phi_{k_n}^*(x')}{\omega - \Omega_n + i\eta} \xrightarrow{x, x' \rightarrow \pm\infty} \frac{1}{2\pi} \int_{0[\text{R}], [\text{L}]}^{\infty} \frac{\phi_k(x)\phi_k^*(x')}{\omega - \Omega_k + i\eta} dk \quad (2.9)$$

In this notation, the functions ϕ_{k_n} are box-normalized, and $\phi_{k_n}(x) = \phi_k(x)/\sqrt{L}$, where $L \rightarrow \infty$ is the length of the box. The transition frequency $\Omega_n = E_n^{N+1} - E_0^{N+1}$ is now simply $\Omega_k = E_0^N + k^2/2 - E_0^{N+1} = k^2/2 + I$, where I is the first ionization potential of the $(N + 1)$ -electron system, and E_0^M and E_n^M are the ground and n^{th} excited state energies of the M -electron system. The subscript “[R],[L]” indicates that the integral is over both orbitals satisfying *right* and *left*

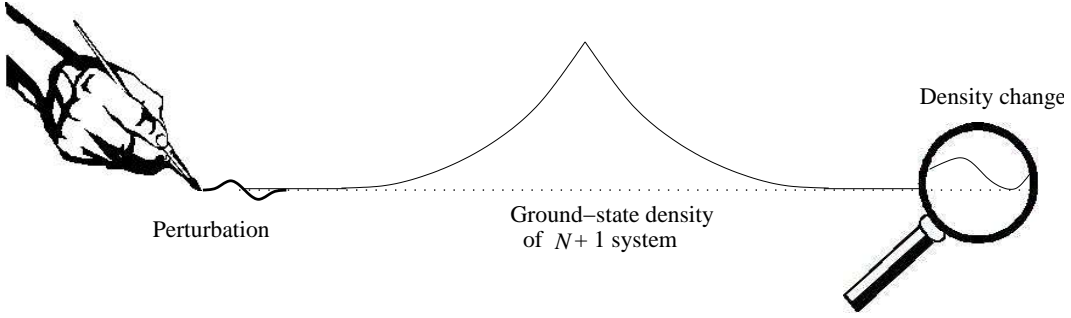


Figure 2.1: Cartoon of Eq.(2.11). To extract the transmission amplitude for an electron of energy ε scattering from an N -electron target: apply a perturbation of frequency $\varepsilon + I$ on the far left of the $(N + 1)$ -ground-state system (I is its first ionization energy), and look at how the density changes oscillate on the far right. Once amplified, the amplitude of these oscillations correspond to $t(\varepsilon)$.

boundary conditions:

$$\phi_k^{\text{[R]}}(x) \rightarrow \begin{cases} e^{\pm ikx} + r_k e^{\mp ikx} & , \quad x \rightarrow \mp\infty \\ t_k e^{\pm ikx} & , \quad x \rightarrow \pm\infty \end{cases} \quad (2.10)$$

When $x \rightarrow -\infty$ and $x' = -x$ the integral of Eq.(2.9) is dominated by a term that oscillates in space with wavenumber $2\sqrt{2(\varepsilon - I)}$ and amplitude given by the transmission amplitude for spin-conserving collisions t_k at that wavenumber (see this explicitly in Appendix A). Denoting this by χ^{osc} , we obtain:

$$t(\varepsilon) = \lim_{x \rightarrow -\infty} \left[\frac{i\sqrt{2\varepsilon}}{\sqrt{\rho(x)\rho(-x)}} \chi^{\text{osc}}(x, -x; \varepsilon + I) \right] . \quad (2.11)$$

Therefore, in order to extract the transmission amplitude $t(\varepsilon)$ from the susceptibility when an electron of energy ε collides with an N -electron target in one dimension, one should first construct the ground-state density of the $(N + 1)$ -electron system, perturb it in the far left with frequency $I + \varepsilon$, and then look at the oscillations of the density change in the far right: the amplitude of these oscillations (“amplified” by $i\sqrt{2\varepsilon}\rho(x)^{-1}$) is the transmission amplitude $t(\varepsilon)$ (see Fig.2.1).

The derivation of Eq.(2.11) does not depend on the interaction between the

electrons. Therefore, the same formula applies to the Kohn-Sham system:

$$t_s(\varepsilon) = \lim_{x \rightarrow -\infty} \left[\frac{i\sqrt{2\varepsilon}}{\sqrt{\rho(x)\rho(-x)}} \chi_s^{\text{osc}}(x, -x; \varepsilon + I) \right] . \quad (2.12)$$

In practice, the Kohn-Sham transmission amplitudes $t_s(\varepsilon)$ are obtained by solving a *potential scattering* problem, i.e., scattering from the $(N + 1)$ -electron ground-state KS potential.

Illustration of Eq.(2.12)

For one electron, the susceptibility is given by [36] (see Appendix C):

$$\chi_s(x, x'; \varepsilon + I) = \sqrt{\rho(x)\rho(x')} [g_s(x, x'; \varepsilon) + g_s^*(x, x'; -\varepsilon - 2I)] , \quad (2.13)$$

where the Green function $g_s(x, x'; \varepsilon)$ has a Fourier transform satisfying

$$\left(-\frac{1}{2} \frac{\partial^2}{\partial x^2} + v_s(x) - i \frac{\partial}{\partial t} \right) g_s(x, x'; t - t') = -i\delta(x - x')\delta(t - t') \quad (2.14)$$

Let's use Eq.(2.12) to find the transmission amplitude for an electron scattering from a double delta-function well, $v_s(x) = -Z_1\delta(x) - Z_2\delta(x - a)$. The Green function can be readily obtained in this case as

$$g_s(x, x') = g_1(x, x') - \frac{Z_2 g_1(x, a) g_1(a, x')}{1 + Z_2 g_1(a, a)} , \quad (2.15)$$

where g_1 is the Green function for a single delta-function of strength Z_1 at the origin. It is given by [37]:

$$g_1(x, x') = \frac{1}{ik} \left(e^{ik|x-x'|} - \frac{Z_1 e^{ik(|x|+|x'|)}}{ik + Z_1} \right) , \quad (2.16)$$

with $k = \sqrt{2\varepsilon}$. We now have all the elements to construct χ_s explicitly. When $x \rightarrow -\infty$ and $x' \rightarrow -x$, its oscillatory part (the coefficient of e^{-2ikx}) multiplied by ik and divided by $\sqrt{\rho(x)\rho(-x)}$ (see Eq.(2.12)) yields

$$t_s = \frac{ik/(Z_1 + ik)}{1 + Z_2 g_1(a, a)} . \quad (2.17)$$

We plot $T_s = |t_s|^2$ in Fig.(2.2).

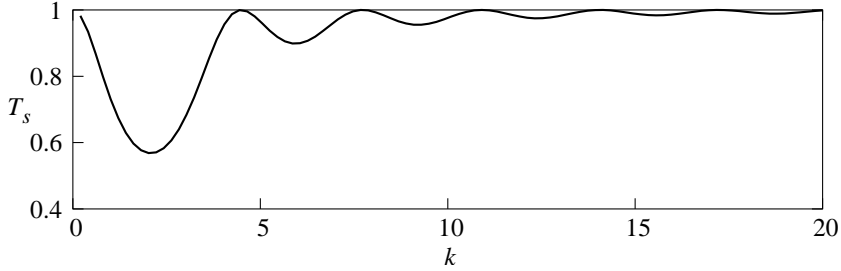


Figure 2.2: Transmission coefficient $T_s = |t_s|^2$ for an electron scattering from the 1d-potential $v_s(x) = -Z_1\delta(x) - Z_2\delta(x - a)$. $Z_1 = Z_2 = 1$ in this plot, and $a = 1$ as well. Interesting: perfect transmission at $k = 0$ due to proximity of the two delta-function wells.

2.2.2 TDDFT equation for transmission amplitudes

The exact amplitudes $t(\varepsilon)$ of the many-body problem are formally related to the $t_s(\varepsilon)$ through Eqs.(2.11), (2.12) and (2.1): the time-dependent response of the $(N + 1)$ -electron ground-state contains the scattering information, and this is accessible via TDDFT. A potential scattering problem is solved first for the $(N + 1)$ -electron ground-state KS potential, and the scattering amplitudes thus obtained (t_s) are further corrected by f_{HXC} to account for, e.g., polarization effects.

Even though Eq.(2.11) is impractical as a basis for computations (one can rarely obtain the susceptibility with the desired accuracy in the asymptotic regions, as we did in the previous example) it leads to practical approximations. The simplest of such approximations is obtained by iterating Eq.(2.1) once, substituting χ by χ_s in the right-hand side of Eq.(2.1). This leads through Eqs.(2.11) and (2.12) to the following useful distorted-wave-Born-type approximation for the transmission amplitude (see Appendix B.4):

$$t(\varepsilon) = t_s(\varepsilon) + \frac{1}{i\sqrt{2\varepsilon}} \langle\langle \text{H}, \varepsilon | \hat{f}_{\text{HXC}}(\varepsilon + I) | \text{H}, \varepsilon \rangle\rangle . \quad (2.18)$$

In Eq.(2.18), the double-bracket notation stands for:

$$\langle\langle \text{H}, \varepsilon | \hat{f}_{\text{HXC}}(\varepsilon + I) | \text{H}, \varepsilon \rangle\rangle = \int \int dx dx' \phi_{\text{H}}(x) \phi_{\varepsilon}^{[\text{L}]}(x) f_{\text{HXC}}(x, x'; \varepsilon + I) \phi_{\text{H}}(x') \phi_{\varepsilon}^{[\text{R}]}(x') , \quad (2.19)$$

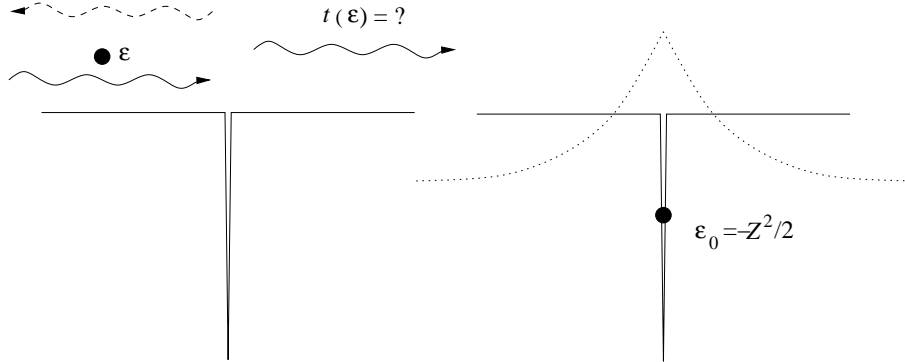


Figure 2.3: Left: cartoon of an electron scattering from a negative delta-function potential. Right: cartoon of an electron bound to the same potential; the ground-state density decays exponentially, just as in hydrogenic ions in 3d.

where ϕ_H is the highest-occupied molecular orbital of the $(N + 1)$ -electron system, and $\phi_\varepsilon^{[R]}(x)$ is the energy-normalized scattering orbital of energy ε satisfying [R]-boundary conditions. This is reminiscent of the single-pole approximation for excitation energies of bound \rightarrow bound transitions [31].

2.2.3 An example, $N = 0$, trivial.

The method outlined above is valid for any number of particles. In particular, for the trivial case of $N = 0$ corresponding to *potential scattering*. Consider again an electron scattering from a negative delta-function of strength Z in one dimension (Fig.(2.3)). The transmission amplitude as a function of ε is given by [38]:

$$t(\varepsilon) = \frac{ik}{Z + ik} \quad , \quad k = \sqrt{2\varepsilon} \quad (2.20)$$

How would TDDFT get this answer?: (1) Find the ground-state KS potential of the $(N + 1) = 1$ -electron system. The external potential admits one bound state of energy $-Z^2/2$. The ground-state KS potential is given by $v_s(x) = v_{\text{ext}}(x) + v_{\text{HXC}}(x)$, but $v_{\text{HXC}} = 0$ for one electron, so $v_s(x) = v_{\text{ext}}(x) = -Z\delta(x)$; (2) Solve Schrödinger's equation for the positive-energy states of an electron in the potential $v_s(x)$, to find $t_s(\varepsilon) = ik/(Z + ik)$. And (3) In this case, $f_{\text{HXC}} = 0$, so $\chi = \chi_s$,

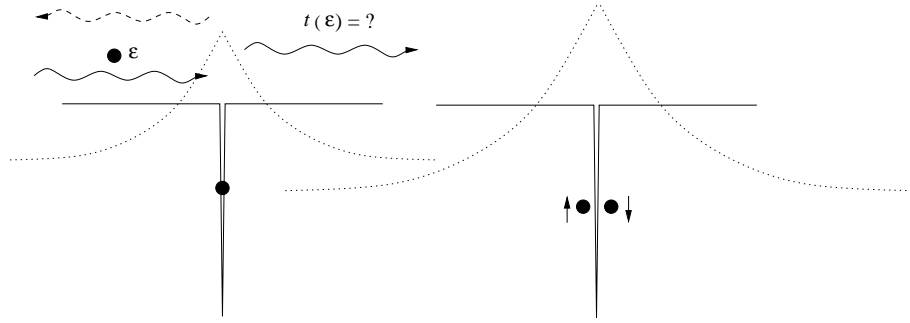


Figure 2.4: Left: cartoon of an electron scattering from 1d-He⁺. Right: cartoon of two electrons bound to the delta function in a singlet state.

and $t = t_s$. Notice that approximations that are not self-interaction corrected (to guarantee $v_{\text{HXC}} = 0$) would give sizable errors in this simple case.

2.2.4 Another example, $N = 1$, not trivial.

Now consider a simple 1-d model of an electron scattering from a one-electron atom of nuclear charge Z [39]:

$$\hat{H} = -\frac{1}{2} \frac{d^2}{dx_1^2} - \frac{1}{2} \frac{d^2}{dx_2^2} - Z\delta(x_1) - Z\delta(x_2) + \lambda\delta(x_1 - x_2) \quad , \quad (2.21)$$

The two electrons interact via a delta-function repulsion, scaled by λ . With $\lambda = 0$ the ground state density is a simple exponential, analogous to hydrogenic atoms in 3d.

(i) Exact solution in the weak interaction limit: First, we solve for the exact transmission amplitudes to first order in λ using the static exchange method [40]. The total energy must be stationary with respect to variations of both the bound (ϕ_b) and scattering (ϕ_s) orbitals that form the spatial part of the Slater determinant: $(\phi_b(x_1)\phi_s(x_2) \pm \phi_b(x_2)\phi_s(x_1)) / \sqrt{2}$, where the upper sign corresponds to the singlet, and the lower sign to the triplet case. The static-exchange equations are:

$$\left[-\frac{1}{2} \frac{d^2}{dx^2} + \gamma |\phi_{s,b}(x)|^2 - Z\delta(x) \right] \phi_{b,s}(x) = \mu_{b,s} \phi_{b,s}(x) \quad , \quad (2.22)$$

where $\gamma = 2\lambda$ for the singlet, and 0 for the triplet. Thus the triplet transmission amplitude is that of a simple δ -function, Eq.(2.20). This can be understood by noting that in the triplet state, the hartree term exactly cancels the exchange (the two electrons only interact when they are at the same place, but they cannot be at the same place when they have the same spin, from Pauli's principle). The results for triplet (t_{trip}) and singlet (t_{sing}) scattering are therefore:

$$\begin{aligned} t_{trip} &= t_0 \quad , \quad t_0 = \frac{ik}{Z + ik} \\ t_{sing} &= t_0 + 2\lambda t_1 \quad , \quad t_1 = \frac{-ik^2}{(k - iZ)^2(k + iZ)} \end{aligned} \quad (2.23)$$

(ii) TDDFT solution: We now show, step by step, the TDDFT procedure yielding the same result, Eqs.(2.23). The first step is finding the ground-state KS potential for two electrons *bound* to the δ -function. The ground-state of the $(N + 1)$ -electron system ($N = 1$) is given to $\mathcal{O}(\lambda)$ by:

$$\Psi_0(x_1\sigma_1, x_2\sigma_2) = \frac{1}{\sqrt{2}}\phi_0(x_1)\phi_0(x_2) [\delta_{\sigma_1\uparrow}\delta_{\sigma_2\downarrow} - \delta_{\sigma_1\downarrow}\delta_{\sigma_2\uparrow}] \quad , \quad (2.24)$$

where the orbital $\phi_0(x)$ satisfies [41, 42]:

$$\left[-\frac{1}{2} \frac{d^2}{dx^2} - Z\delta(x) + \lambda|\phi_0(x)|^2 \right] \phi_0(x) = \mu\phi_0(x) \quad (2.25)$$

To first order in λ ,

$$\phi_0(x) = \sqrt{Z}e^{-Z|x|} + \frac{\lambda}{8\sqrt{Z}} \left(2e^{-3Z|x|} + e^{-Z|x|}(4Z|x| - 3) \right) \quad (2.26)$$

The bare KS transmission amplitudes $t_s(\varepsilon)$ characterize the asymptotic behavior of the continuum states of $v_s(x) = -Z\delta(x) + \lambda|\phi_0(x)|^2$, and can be obtained to $\mathcal{O}(\lambda)$ by a distorted-wave Born approximation (see e.g. Ref.[43]):

$$t_s = t_0 + \lambda t_1 \quad (2.27)$$

The result is plotted in Fig.(2.5), along with the interacting singlet and triplet transmission amplitudes, Eqs.(2.23). The quantity λt_1 is the *error* of the ground-state calculation. The interacting problem cannot be reduced to scattering from

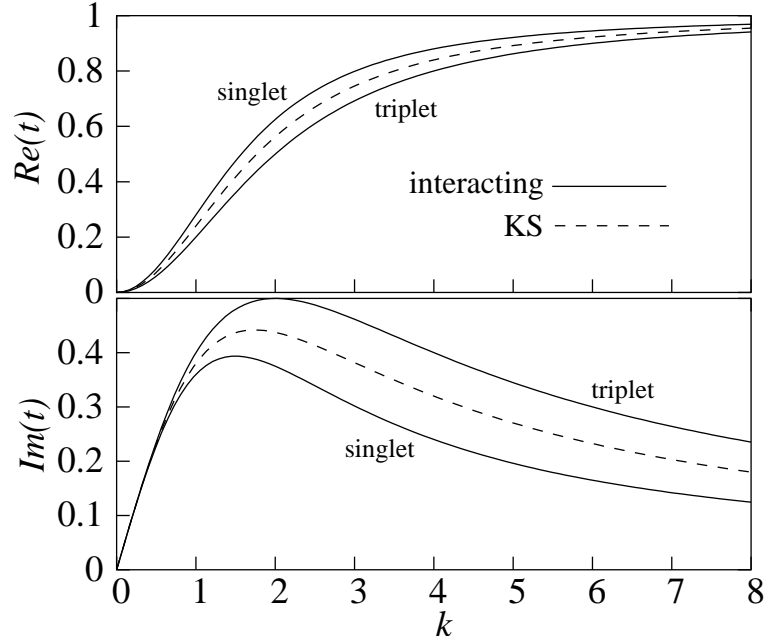


Figure 2.5: Real and imaginary parts of the KS transmission amplitude t_s , and of the interacting singlet and triplet amplitudes, for the model system of Eq.(2.21). $Z = 2$ and $\lambda=0.5$ in this plot.

the $(N + 1)$ -KS potential, but this is certainly a good starting point; in this case, the KS transmission amplitudes are the exact average of the true singlet and triplet amplitudes (compare Eq.(2.27) with Eq.(2.23)).

We now apply Eq.(2.11) to show that the f_{HXC} -term of Eq.(2.1) corrects the t_s values to their exact singlet and triplet amplitudes. The kernel f_{HXC} is only needed to $\mathcal{O}(\lambda)$:

$$f_{\text{HX}}^{\sigma\sigma'}(x, x'; \omega) = \lambda\delta(x - x')(1 - \delta_{\sigma\sigma'}) \quad , \quad (2.28)$$

where the f_{HXC} of Eq.(2.1) is given to $\mathcal{O}(\lambda)$ by $f_{\text{HX}} = f_{\text{H}} + f_{\text{X}} = \frac{1}{4} \sum_{\sigma\sigma'} f_{\text{HX}}^{\sigma\sigma'}$ ($= \frac{1}{2}f_{\text{H}}$ here; for the details, see Appendix D). Eq.(2.28) yields:

$$\chi(x, x'; \omega) = \chi_s(x, x'; \omega) + \frac{\lambda}{2} \int dx'' \chi_s(x, x''; \omega) \chi(x'', x'; \omega) \quad (2.29)$$

Since the ground state of the 2-electron system is a spin-singlet, the Kronecker delta δ_{S_0, S_n} in Eq.(2.8) implies that only *singlet* scattering information may be

extracted from χ , whereas information about triplet scattering requires the magnetic susceptibility $\mathcal{M} = \sum_{\sigma\sigma'}(\sigma\sigma')\chi_{\sigma\sigma'}$, related to the KS susceptibility by spin-TDDFT [44] (see Appendix D):

$$\mathcal{M}(x, x'; \omega) = \chi_s(x, x'; \omega) - \frac{\lambda}{2} \int dx'' \chi_s(x, x''; \omega) \mathcal{M}(x'', x'; \omega) \quad (2.30)$$

For either singlet or triplet case, since the correction to χ_s is multiplied by λ , the leading correction to $t_s(\varepsilon)$ is determined by the same quantity, $\hat{\chi}_s^{(0)} * \hat{\chi}_s^{(0)}$, where $\hat{\chi}_s^{(0)}$ is the 0th order approximation to the KS susceptibility (i.e. with $v_s(x) = v_s^{(0)}(x) = -Z\delta(x)$). Its oscillatory part at large distances [36] (multiplied by $\sqrt{\rho(x)\rho(-x)}/ik$, see Eq.(2.11)) is precisely equal to λt_1 . We then find through Eqs.(2.11), (2.29), and (2.30) that

$$t_{sing} = t_s + \lambda t_1 \quad , \quad t_{trip} = t_s - \lambda t_1 \quad , \quad (2.31)$$

in agreement with Eqs.(2.23).

The method illustrated in the preceding example is applicable to any one-dimensional scattering problem. Eqs.(2.11) and (2.1) provide a way to obtain scattering information for an electron that collides with an N -electron target *entirely* from the $(N + 1)$ -electron ground-state KS susceptibility (and a given approximation to f_{xc}).

2.3 Three dimensions

2.3.1 Single Pole Approximation in the continuum

Here we derive an analog of Eq.(2.18) in 3d. Consider the $l = 0$ Rydberg series of bound states converging to the first ionization threshold I of the $(N + 1)$ -electron system:

$$E_n - E_0 = I - 1/ \left[2(n - \mu_n)^2 \right] \quad , \quad (2.32)$$

where μ_n is the quantum defect of the n^{th} excited state. Let

$$\epsilon_n = -1/ [2(n - \mu_{s,n})^2] \quad (2.33)$$

be the KS orbital energies of that series. The true transition frequencies $\omega_n = E_n - E_0$, are related through TDDFT to the KS frequencies $\omega_{s,n} = \epsilon_n - \epsilon_{\text{H}}$, where ϵ_{H} is the HOMO energy. Within the single-pole approximation (SPA) [31],[45]:

$$\omega_n = \omega_{s,n} + 2\langle\langle_{\text{HOMO}}, n | \hat{f}_{\text{HXC}}(\omega_n) |_{\text{HOMO}}, n \rangle\rangle \quad (2.34)$$

Numerical studies [46] suggest that $\Delta\mu_n = \mu_n - \mu_{s,n}$ is a small number when $n \rightarrow \infty$. Expanding ω_n around $\Delta\mu_n = 0$, and using $I = -\epsilon_{\text{H}}$, we find:

$$\omega_n = \omega_{s,n} - \frac{\Delta\mu_n}{(n - \mu_{s,n})^3} \quad (2.35)$$

We conclude that, within the SPA,

$$\Delta\mu_n = -2(n - \mu_{s,n})^3 \langle\langle_{\text{HOMO}}, n | \hat{f}_{\text{HXC}}(\omega_n) |_{\text{HOMO}}, n \rangle\rangle. \quad (2.36)$$

Letting $n \rightarrow \infty$, Seaton's theorem ($\pi \lim_{n \rightarrow \infty} \mu_n = \delta(\varepsilon \rightarrow 0^+)$)[47] implies:

$$\delta(\varepsilon) \stackrel{\text{SPA}}{=} \delta_s(\varepsilon) - 2\pi \langle\langle_{\text{HOMO}}, \varepsilon | \hat{f}_{\text{HXC}}(\varepsilon + I) |_{\text{HOMO}}, \varepsilon \rangle\rangle \quad (2.37)$$

a relation for the phase-shifts δ in terms of the KS phase-shifts δ_s applicable when $\varepsilon \rightarrow 0^+$. The factor $(n - \mu_{s,n})^3$ of Eq.(2.36) gets absorbed into the energy-normalization factor of the KS continuum states.

We illustrate in Fig.(2.6) the remarkable accuracy of Eq.(2.37) when applied to the case of electron scattering from He^+ . For this system, an essentially exact ground-state potential for the $N = 2$ -electron system is known. This was found by inverting the KS equation using the ground-state density of an extremely accurate wavefunction calculation of the He atom [48]. We calculated the low-energy KS s -phase shifts from this potential, $\delta_s(\varepsilon)$ (dashed line in the center, Fig.(2.6)), and then corrected these phase shifts according to Eq.(2.37) employing the BPG approximation to f_{HXC} [49] (= adiabatic local density approximation for

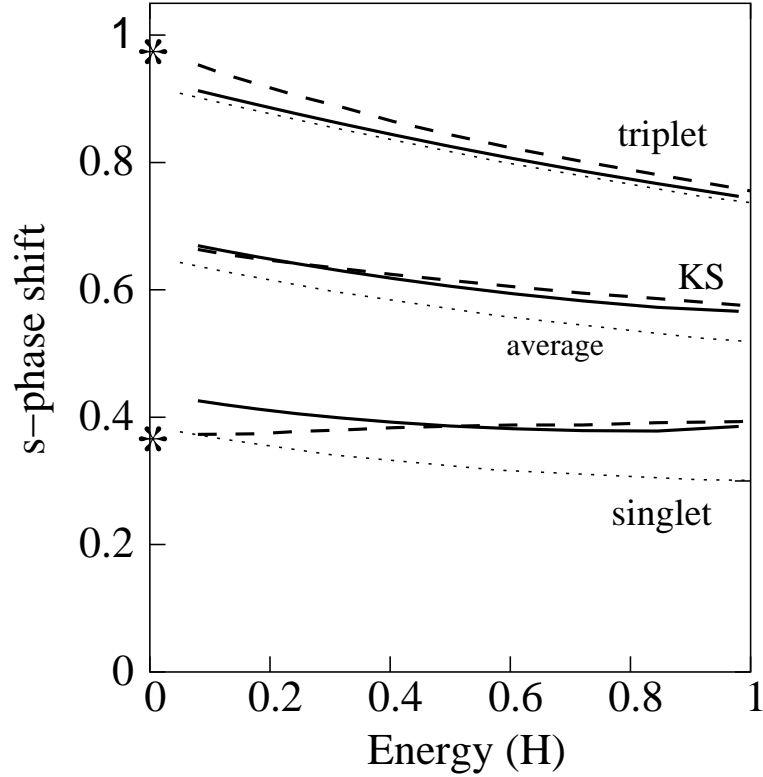


Figure 2.6: s -phase shifts as a function of energy for electron scattering from He^+ . *Dashed lines*: the line labeled KS corresponds to the phase shifts from the *exact* KS potential of the He atom; the other dashed lines correspond to the TDDFT singlet and triplet phase shifts calculated in the present work according to Eq.(2.37). *Solid lines*: accurate wavefunction calculations of electron- He^+ scattering from Ref.[50]. The solid line in the center is the average of singlet and triplet phase shifts. *Dotted lines*: Static exchange calculations, from Ref.[51]. The asterisks at zero energy correspond to extrapolating the bound \rightarrow bound results of Ref.[49].

antiparallel contribution to f_{HXC} and exchange-only approximation for the parallel contribution. See Appendix E for details on the numerical calculation). We also plot the results of a highly accurate wavefunction calculation [50] (solid), and of static-exchange calculations [51] (dotted). The results show that phase shifts from the $(N+1)$ -electron ground-state KS potential, $\delta_s(\varepsilon)$, are excellent approximations to the average of the true singlet/triplet phase shifts for an electron scattering from the N -electron target, just as in the one-dimensional model of the previous section; they also show that TDDFT, with existing approximations, works very well to correct scattering from the KS potential to the true scattering phase shifts, at least at low energies. In fact, for the singlet phase shifts, TDDFT does better than the computationally more demanding static exchange method, and for the triplet case TDDFT does only slightly worse. Even though Eq.(2.37) is, strictly speaking, only applicable at zero energy (marked with asterisks in Fig.(2.6)), it clearly provides a good description for finite (low) energies. It is remarkable that the antiparallel spin kernel, which is completely local in space and time, and whose value at each point is given by the exchange-correlation energy density of a uniform electron gas (evaluated at the ground-state density at that point), yields phase shifts for e-He⁺ scattering with less than 20% error. Since a signature of density-functional methods is that with the same functional approximations, exchange-correlation effects are often better accounted for in larger systems, the present approach holds promise as a practical method for studying scattering from large targets.

2.3.2 Partial-wave analysis of scattering within TDDFT

In the previous subsection we derived a single-pole approximation for bound \rightarrow continuum transitions by extrapolating the well-known single-pole approximation corresponding to bound \rightarrow bound transitions. We will now go to the other side of the threshold, and focus on the TDDFT linear response at frequencies which

are higher than the ionization potential of the $(N + 1)$ -electron system.

Linear response equation at large distances

We restrict the discussion to spherically symmetric $(N + 1)$ -electron systems. In such cases, the Green function $g_s(\mathbf{r}, \mathbf{r}'; \omega)$ that builds up the KS susceptibility

$$\chi_s(\mathbf{r}, \mathbf{r}'; \omega) = 2 \sum_{i \text{ occ}} \phi_i^*(\mathbf{r}) \phi_i(\mathbf{r}') g_s(\mathbf{r}, \mathbf{r}'; \epsilon_i + \omega) + c.c.(\omega \rightarrow -\omega) \quad , \quad (2.38)$$

can be expanded in spherical harmonics as:

$$g_s(\mathbf{r}, \mathbf{r}'; \omega) = \sum_{l=0}^{\infty} \sum_{m=-l}^l g_{sl}(r, r'; \epsilon_i + \omega) Y_l^m(\hat{\mathbf{r}}) Y_l^{m*}(\hat{\mathbf{r}}') \quad . \quad (2.39)$$

Introduce the shorthand notation $\mathcal{Y}_{lm}^{\hat{\mathbf{r}}\hat{\mathbf{r}}'} \equiv Y_l^m(\hat{\mathbf{r}}) Y_l^{m*}(\hat{\mathbf{r}}')$. When the magnitude of one of the arguments of $\chi_s(\mathbf{r}, \mathbf{r}'; \omega)$ is very large, say $r \rightarrow \infty$, then

$$\chi_s(\mathbf{r}, \mathbf{r}'; \omega) \xrightarrow{r \rightarrow \infty} \frac{2\sqrt{\rho(r)} u_{sH}(r')}{r r'} \mathcal{Y}_{l_H m_H}^{*\hat{\mathbf{r}}\hat{\mathbf{r}}'} \sum_{l,m} g_{sl}(r, r'; \omega - I) \mathcal{Y}_{lm}^{\hat{\mathbf{r}}\hat{\mathbf{r}}'} \quad , \quad (2.40)$$

where $u_{sH}(r)$ stands for the *radial* KS HOMO, i.e. $\phi_{sH}(\mathbf{r}) = r^{-1} u_{sH}(r) Y_{l_H}^{m_H}(\hat{\mathbf{r}})$. We have dropped the $c.c.(\omega \rightarrow -\omega)$ term because χ_s is dominated by the exponential decay of $g_s^*(\omega \rightarrow -\omega)$ at large distances, in addition to that of the density. We will also need the limiting form of the susceptibility when the magnitudes of *both* arguments, r and r' , are very large. As $r' \rightarrow \infty$ ($r' < r$), Eq.(2.40) becomes

$$\chi_s(\mathbf{r}, \mathbf{r}'; \omega) \xrightarrow{r > r' \rightarrow \infty} \frac{2\sqrt{\rho(r)\rho(r')}}{r r'} \mathcal{Y}_{l_H m_H}^{*\hat{\mathbf{r}}\hat{\mathbf{r}}'} \sum_{l,m} g_{sl}(r, r'; \omega - I) \mathcal{Y}_{lm}^{\hat{\mathbf{r}}\hat{\mathbf{r}}'} \quad . \quad (2.41)$$

We keep $r > r'$ to facilitate the discussion that follows, but $r' \geq r$ leads to the same results. We now state without proof that the susceptibility of the interacting system has the analogous behavior:

$$\chi(\mathbf{r}, \mathbf{r}'; \omega) \xrightarrow{r \rightarrow \infty} \frac{2\sqrt{\rho(r)} u_H(r')}{r r'} \mathcal{Y}_{l_H m_H}^{*\hat{\mathbf{r}}\hat{\mathbf{r}}'} \sum_{l,m} g_l(r, r'; \omega - I) \mathcal{Y}_{lm}^{\hat{\mathbf{r}}\hat{\mathbf{r}}'} \quad , \quad (2.42)$$

where $g_l(r, r'; \omega)$ is the radial interacting Green function of the $(N + 1)$ -electron system, and $u_H(r')$ is a function of r' only, which becomes equal to $u_{sH}(r')$ as

$r' \rightarrow \infty$ and is defined by Eq.(2.42) itself. When both r and r' go to infinity:

$$\chi(\mathbf{r}, \mathbf{r}'; \omega) \xrightarrow{r > r' \rightarrow \infty} \frac{2\sqrt{\rho(r)\rho(r')}}{rr'} \mathcal{Y}_{l_H m_H}^{*\hat{\mathbf{r}}\hat{\mathbf{r}}'} \sum_{l,m} g_l(r, r'; \omega - I) \mathcal{Y}_{lm}^{\hat{\mathbf{r}}\hat{\mathbf{r}}'} . \quad (2.43)$$

Now insert Eqs.(2.40)-(2.43) into the TDDFT linear response formula when $r > r' \rightarrow \infty$:

$$\lim_{r > r' \rightarrow \infty} \chi(\mathbf{r}, \mathbf{r}'; \omega) = \lim_{r > r' \rightarrow \infty} \chi_s(\mathbf{r}, \mathbf{r}'; \omega) + 2 \lim_{r > r' \rightarrow \infty} \int d\mathbf{r}_1 d\mathbf{r}_2 \chi_s(\mathbf{r}, \mathbf{r}_1; \omega) f_{\text{HXC}}(\mathbf{r}_1, \mathbf{r}_2; \omega) \chi(\mathbf{r}_2, \mathbf{r}'; \omega) . \quad (2.44)$$

Multiplying throughout by $\mathcal{Y}_{LM}^{*\hat{\mathbf{r}}\hat{\mathbf{r}}'} = Y_L^{M*}(\Omega) Y_L^M(\Omega')$, integrating over the solid angles $d\Omega$ and $d\Omega'$ to project out the (L, M) -component, and setting $(L, M) \rightarrow (l, m)$, we get the integral equation

$$\begin{aligned} \lim_{r > r' \rightarrow \infty} g_l(r, r'; \varepsilon) &= \lim_{r > r' \rightarrow \infty} g_{sl}(r, r'; \varepsilon) + 2 \lim_{r > r' \rightarrow \infty} \int d\mathbf{r}_1 \int d\mathbf{r}_2 \frac{u_{\text{SH}}(r_1) u_{\text{H}}(r_2)}{r_1 r_2} \times \\ &\quad \times g_{sl}(r, r_1; \varepsilon) f_{\text{HXC}}(\mathbf{r}_1, \mathbf{r}_2; \varepsilon + I) g_l(r_2, r'; \varepsilon) \mathcal{Y}_{l_H m_H}^{\hat{\mathbf{r}}_1 \hat{\mathbf{r}}_2} \mathcal{Y}_{l_0}^{*\hat{\mathbf{r}}_1 \hat{\mathbf{r}}_2} \end{aligned} \quad (2.45)$$

where $\varepsilon = \omega - I > 0$ is the energy of the projectile electron.

Asymptotic behavior of Green functions

The radial KS Green function $g_{sl}(r, r'; \varepsilon)$ can be written as ([43],[52]):

$$g_{sl}(r, r'; \varepsilon) = -2 (rr' W_s)^{-1} u_{skl}^{(1)}(r_<) u_{skl}^{(2)}(r_>) , \quad (2.46)$$

where $u_{skl}^{(1)}(r)$ solves the radial Schrödinger equation with the ground-state KS potential $v_s(r)$:

$$\left(\frac{d^2}{dr^2} + k^2 - 2v_s(r) - \frac{l(l+1)}{r^2} \right) u_{skl}(r) = 0 , \quad (2.47)$$

and is regular at the origin: $u_{skl}^{(1)}(0) = 0$. It has the asymptotic behavior:

$$u_{skl}^{(1)}(r) \xrightarrow{r \rightarrow \infty} k^{-1} e^{i\delta_{sl}} \sin(h_{kl}(r) + \delta_{sl}) \quad (2.48)$$

where

$$h_{kl}(r) = kr - l\pi/2 + \gamma \left[\frac{1}{k} \ln 2kr + \sigma_l \right] . \quad (2.49)$$

The value of γ depends on whether $v_s(r)$ is long-ranged ($\gamma = 1$) or short-ranged ($\gamma = 0$); the Kohn-Sham phase shifts δ_{sl} are the phase shifts of the radial orbitals in addition to the σ_l due to scattering from a pure Coulomb potential.

The orbital $u_{skl}^{(2)}(r)$ of Eq.(2.46) is an irregular solution of Eq.(2.47), with asymptotic behavior:

$$u_{skl}^{(2)}(r) \xrightarrow{r \rightarrow \infty} k^{-1} e^{i(h_{kl}(r) + 2\delta_{sl})} . \quad (2.50)$$

In Eq.(2.46), $W_s = k^{-1} \exp(2i\delta_{sl})$ is the Wronskian between $u_{skl}^{(1)}$ and $u_{skl}^{(2)}$.

In order to obtain scattering information from Eq.(2.45), we need the KS Green function when $r \rightarrow \infty$:

$$g_{sl}(r, r'; \varepsilon) \xrightarrow{r \rightarrow \infty} -2(rr')^{-1} e^{ih_{kl}(r)} u_{skl}^{(1)}(r') , \quad (2.51)$$

as well as when both r and r' go to infinity:

$$g_{sl}(r, r'; \varepsilon) \xrightarrow{r > r' \rightarrow \infty} -2(krr')^{-1} e^{i(h_{kl}(r) + \delta_{sl})} \sin(h_{kl}(r') + \delta_{sl}) . \quad (2.52)$$

We also need $g_l(r, r')$ in these two limits. With all likelihood:

$$g_l(r, r'; \varepsilon) \xrightarrow{r \rightarrow \infty} -2(rr')^{-1} e^{ih_{kl}(r)} u_{kl}^{(1)}(r') \quad (2.53)$$

$$g_l(r, r'; \varepsilon) \xrightarrow{r > r' \rightarrow \infty} -2(krr')^{-1} e^{i(h_{kl}(r) + \delta_l)} \sin(h_{kl}(r') + \delta_l) , \quad (2.54)$$

where the definition of $u_{kl}(r')$ is that of Eq.(2.53), and the δ_l are the *exact* l -phase shifts of the interacting scattering problem.

Notice that inserting Eqs.(2.51)-(2.54) into Eq.(2.45), the r -dependence drops out completely, yielding ($r' \rightarrow r$):

$$e^{i\delta_l} \sin(h_{kl}(r) + \delta_l) = e^{i\delta_{sl}} \sin(h_{kl}(r) + \delta_{sl}) - 4k e^{ih_{kl}(r)} \langle\langle f_{\text{HXC}} \rangle\rangle_l , \quad (2.55)$$

where

$$\langle\langle f_{\text{HXC}} \rangle\rangle_l = \int d\mathbf{r}_1 \int d\mathbf{r}_2 \frac{u_{s\text{H}}(r_1) u_{\text{H}}(r_2)}{(r_1 r_2)^2} u_{skl}^{(1)}(r_1) f_{\text{HXC}}(\mathbf{r}_1, \mathbf{r}_2; \varepsilon + I) u_{kl}^{(1)}(r_2) \mathcal{Y}_{l\text{H}m\text{H}}^{\hat{\mathbf{r}}_1 \hat{\mathbf{r}}_2} \mathcal{Y}_{l0}^{*\hat{\mathbf{r}}_1 \hat{\mathbf{r}}_2} . \quad (2.56)$$

To understand the significance of Eq.(2.55), consider the Lippmann-Schwinger equation for a two-potential scattering problem [52], where an electron scatters from $v_s(r) + v_1(r)$, the sum of two potentials. The k -scattering solution in this potential is given by:

$$u_{kl}(r) = u_{skl}^{(1)}(r) + \int_0^\infty dr' g_{sl}(r, r'; k^2/2) v_1(r') u_{kl}(r') . \quad (2.57)$$

With the asymptotic forms given in Eqs.(2.48) and (2.51), we see that

$$k u_{kl}(r) \xrightarrow{r \rightarrow \infty} e^{i\delta_{sl}} \sin(h_{kl}(r) + \delta_{sl}) - 2k e^{ih_{kl}(r)} \int_0^\infty dr' u_{skl}^{(1)}(r') v_1(r') u_{kl}(r') . \quad (2.58)$$

Therefore, Eq.(2.55) is *almost* Lippmann-Schwinger's equation at large distances. If electrons were contact-interacting in such a way that f_{HXC} were proportional to $f_{\text{HXC}}^{\text{approx}}(r)\delta(\mathbf{r} - \mathbf{r}')$ then Eq.(2.55) would be precisely Lippmann-Schwinger's equation (at large distances) provided we identified $v_1(r)$ with:

$$v_1(r) = 2u_{s\text{H}}(r)u_{\text{H}}(r)f_{\text{HXC}}^{\text{approx}}(r)u_{skl}^{(1)}(r) \int d\Omega \mathcal{Y}_{l\text{H}m\text{H}}^{\hat{\mathbf{r}}} \mathcal{Y}_{l0}^{*\hat{\mathbf{r}}} . \quad (2.59)$$

The correlation contribution to f_{HXC} in ALDA, for example, is of such form.

TDDFT equation for t -matrix elements and phase shifts

With the usual definition of the *transition matrix* in the angular momentum representation [52]:

$$t_l \equiv -\frac{1}{k} e^{i\delta_l} \sin \delta_l , \quad (2.60)$$

Eq.(2.55) leads, after some algebra, to:

$$t_l = t_{sl} + 4\langle\langle f_{\text{HXC}} \rangle\rangle_l , \quad (2.61)$$

where $t_{sl} = -k^{-1} \exp(i\delta_{sl}) \sin \delta_{sl}$. It is remarkable that, if assumptions (2.42) and (2.53) are true, the simple expression of Eq.(2.61) is in fact *exact*.

Now suppose that $\delta_l^{(1)} = \delta_l - \delta_{sl}$ is a small quantity, and expand Eq.(2.61) to first order in $\delta_l^{(1)}$, just as we did in the previous subsection for the quantum

defects of Rydberg transitions. We find:

$$\delta_l = \delta_{sl} - 4ke^{(-2i\delta_{sl})} \langle \langle f_{\text{HXC}} \rangle \rangle_l . \quad (2.62)$$

Finally, approximate

$$u_{\text{H}}(r) \sim u_{s_{\text{H}}}(r) , \quad u_{kl}^{(1)}(r) \sim u_{skl}^{(1)}(r) , \quad (2.63)$$

and impose energy-normalization by requiring that the scattering orbitals go asymptotically like [43]

$$\tilde{u}_{skl}^{(1)} = \sqrt{\frac{2k}{\pi}} e^{-i\delta_{sl}} u_{skl}^{(1)}(r) \xrightarrow{r \rightarrow \infty} \sqrt{\frac{2}{\pi k}} \sin(h_{kl}(r) + \delta_{sl}) . \quad (2.64)$$

Eq.(2.62) can then be re-written as:

$$\delta_l = \delta_{sl} - 2\pi [[f_{\text{HXC}}]]_l^{\text{B.A.}} \quad (2.65)$$

$$[[f_{\text{HXC}}]]_l^{\text{B.A.}} \equiv \int d\mathbf{r}_1 \int d\mathbf{r}_2 \frac{u_{s_{\text{H}}}(r_1) u_{s_{\text{H}}}(r_2) \tilde{u}_{skl}^{(1)}(r_1) \tilde{u}_{skl}^{(1)}(r_2)}{(r_1 r_2)^2} f_{\text{HXC}}(\mathbf{r}_1, \mathbf{r}_2; \varepsilon + I) \mathcal{Y}_{lH}^{\hat{\mathbf{r}}_1 \hat{\mathbf{r}}_2} \mathcal{Y}_{l0}^{*\hat{\mathbf{r}}_1 \hat{\mathbf{r}}_2} , \quad (2.66)$$

with the superscript ‘‘B.A.’’ standing for Born-type approximation. Eq.(2.65) coincides with the SPA formula derived via quantum-defect theory in the previous subsection, Eq.(2.37).

2.4 Summary and outlook

Based on the linear response formalism of TDDFT we have discussed a new way of calculating elastic scattering amplitudes for electrons scattering from targets that can bind an extra electron. In one dimension, transmission amplitudes can be extracted from the $(N + 1)$ -electron ground-state susceptibility, as indicated by Eq.(2.11). Since the susceptibility of the interacting system is determined by the Kohn-Sham susceptibility within a given approximation to the exchange-correlation kernel, Eq.(2.1), the transmission amplitudes of the interacting system

can be obtained by appropriately correcting the bare Kohn-Sham scattering amplitudes. Eq.(2.18), reminiscent of the single-pole approximation for bound \rightarrow bound transitions, provides the simplest approximation to such a correction. A similar formula for scattering phase shifts near zero energy, Eq.(2.37), was obtained in three dimensions by applying concepts of quantum defect theory. Finally, a simple expression for the angular representation of t -matrix elements, Eq.(2.61) was derived for the case of $(N + 1)$ -electron systems that have a spherically symmetric KS potential.

These constitute first steps towards the ultimate goal, which is to accurately treat bound-free correlation for low-energy electron scattering from polyatomic molecules. An obvious limitation of the present approach is that it can only be applied to targets that bind an extra electron because the starting point is always the $(N + 1)$ -ground-state Kohn-Sham system, which may not exist if the N -electron target is neutral, and certainly does not exist if the target is a negative ion. In addition to extending the formalism to treat such cases, there is much work yet to be done: a general proof of principle in three dimensions, testing the accuracy of approximate ground-state KS potentials, developing and testing approximate solutions to the TDDFT Dyson-like equation, extending the formalism to inelastic scattering, etc. Thus, there is a long and winding road connecting the first steps presented here with the calculations of accurate cross sections for electron scattering from large targets when bound-free correlations are important. The present results show that this road is promising.

Chapter 3

Accurate Rydberg excitations from the Local Density Approximation

The Local Density Approximation (LDA) is the simplest and historically most successful approximation in Density Functional Theory [6]. It was proposed by Kohn and Sham [4] soon after the ground-breaking paper of Hohenberg and Kohn [3]. Whereas new generations of functionals have achieved better accuracy than LDA for many properties, its ratio of reliability to simplicity has no paragon. The LDA approximates the exchange-correlation contribution to the ground-state energy by

$$E_{\text{xc}}^{\text{LDA}}[\rho] = \int d\mathbf{r} \rho(\mathbf{r}) \varepsilon_{\text{xc}}^{\text{unif}}(\rho(\mathbf{r})) \quad , \quad (3.1)$$

where $\varepsilon_{\text{xc}}^{\text{unif}}(\rho)$ is the exchange-correlation energy per particle in a uniform electron gas of density ρ . Eq.(3.1) yields the *exact* exchange-correlation energy for this system (the uniform electron gas), because $E_{\text{xc}}[\rho] = N\varepsilon_{\text{xc}}^{\text{unif}}(\rho)$ in this case, where N is the number of electrons. As Kohn and Sham put it in their 1965 paper [4], “Our sole approximation consists of assuming that Eq.(3.1) constitutes an adequate representation of exchange and correlation effects in the systems under consideration”, that is, inhomogeneous systems. Although the LDA yields useful approximations to the total energy of atoms and molecules, the corresponding ground-state KS potentials are poor approximations [53] to the exact ones. In particular, the LDA (or GGA) potential of a neutral atom decays exponentially at large distances, rather than as $-1/r$ as the exact KS potential does. This is because within the LDA, the Hartree potential correctly cancels the external

potential at large distances but the exchange-correlation potential incorrectly decays exponentially:

$$v_{\text{XC}}^{\text{LDA}}(\mathbf{r}) \equiv \frac{\delta E_{\text{XC}}^{\text{LDA}}[\rho]}{\delta \rho(\mathbf{r})} = \varepsilon_{\text{XC}}^{\text{unif}}(\rho(\mathbf{r})) + \rho(\mathbf{r}) \left. \frac{\partial \varepsilon_{\text{XC}}^{\text{unif}}(\rho)}{\partial \rho} \right|_{\rho=\rho(\mathbf{r})}, \quad (3.2)$$

since the density itself decays exponentially. As a result, the LDA potential for an atom does not support a Rydberg series of bound states. The first ionization threshold in the optical spectrum is at the magnitude of the energy of the highest occupied atomic orbital: In an LDA or GGA calculation this is typically too small by several eV. These approximate potentials have excitations to the continuum at frequencies where Rydberg excitations occur in the exact potential. This led many researchers to believe that excitations into Rydberg states cannot be treated at all within LDA (or GGA), or that the only way to do so is by asymptotically correcting the potentials [54]-[58]. Exact exchange (OEP) potentials [59, 60] decay correctly, but at significant additional computational cost. At the same time, there has been a proliferation of real-time TDLDA calculations of electronic excitations of molecules and clusters, and even solids (see Ref.[29] for examples). These evolve the time-dependent Kohn-Sham equations under a weak perturbation, and extract the time-dependent dipole moment of the target. Fourier transform yields the optical intensity as a function of frequency. Such calculations often yield remarkably useful results, but, due to truncation after a large but finite time, often do not carefully distinguish bound-bound from bound-free transitions. Based on the above reasoning, authors usually downplay the significance of their own results beyond the LDA threshold [61]-[64]. This prognosis is unnecessarily bleak. In fact, TDLDA yields accurate optical spectra, even near the ionization threshold. Fig.(3.1) shows this for the neon atom. The oscillator strengths associated with exact Rydberg excitations remain in the same frequency region in LDA (even though the Rydberg states themselves are missing), as suggested by Zangwill and Soven [65, 66], and confirmed numerically by Zangwill [67] for the krypton atom, where the TDLDA *continuum* absorption in

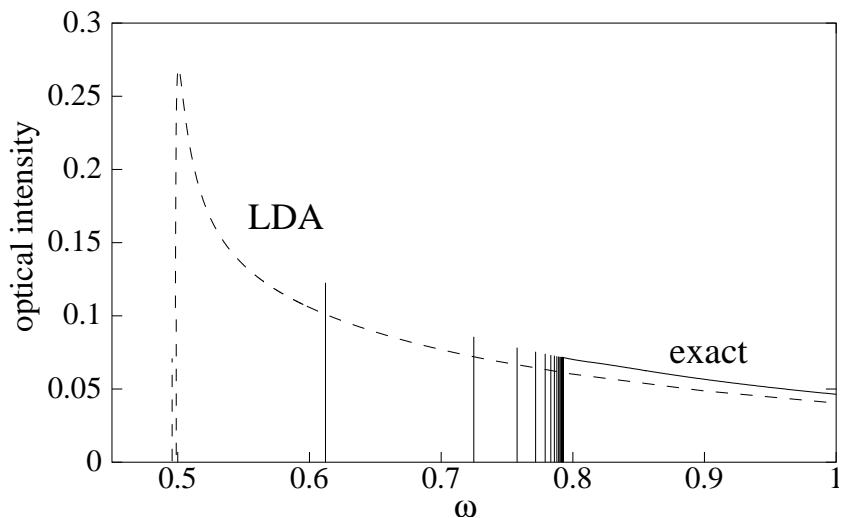


Figure 3.1: Oscillator strengths (in inverse Hartrees) for the $2p \rightarrow ns$ transitions in Ne as a function of photon energy (in Hartrees), from the exact KS potential, and from the LDA one. The discrete spectrum has been multiplied by the density-of-states factor (see text).

the range 10-14 eV was found to agree with the experimental *discrete* absorption within 5%. We explain why this is true for most atomic and molecular systems.

In Section 3.1 we focus on oscillator strengths, showing that the LDA photoionization intensities are good approximations to the true Rydberg photoabsorption intensities. In Section 3.2 we go further, showing how the low-energy LDA scattering states can in fact tell us the position of the true Rydberg excitations.

3.1 Rydberg oscillator strengths from LDA scattering states

3.1.1 Truncated and shifted Coulomb potential

First, consider the hydrogen atom potential, $V(r) = -1/r$. Now shift the potential upwards by a small amount C , and truncate it when it reaches zero, i.e.

$$V_{tr}(r) = \begin{cases} -1/r + C, & r \leq 1/C \\ 0, & r > 1/C \end{cases} \quad (3.3)$$

Since this potential does not decay as $-1/r$ at large distances, it does not support a Rydberg series. Its ionization potential is red-shifted by about C . In Fig.(3.2), we plot the optical intensity of both the pure and truncated Coulomb potentials in the vicinity of the ionization threshold, for $C = 1/20$ (1.35 eV). The discrete transitions have optical intensity $F_{fi}\delta(\omega - \omega_{fi})$, where ω_{fi} is the transition frequency and F_{fi} is its oscillator strength:

$$F_{fi} = \frac{2\omega_{fi}}{3} \frac{l_{>}}{2l_i + 1} \left(\int_0^\infty dr \phi_f(r) r \phi_i(r) \right)^2. \quad (3.4)$$

Here ϕ_i and ϕ_f are the initial and final radial orbitals, and $l_{>}$ is the larger of l_i and l_f . However, for reasons explained below, we represent them by single lines of height $n^3 F_{fi}$, where n is the radial quantum number of the final state. The similarity between the two curves is striking, both above the exact threshold and between the two ionization thresholds. As long as $1/C$ is not too close to the nucleus, this behavior is observed for any value of C .

The phenomenon is well-known in atomic physics [43]. The two potentials differ only by a constant, except at large r ($> 1/C$). Their ground-state orbitals are virtually identical. The Rydberg states of the pure Coulombic potential are also almost identical to the *continuum* states of the shifted potential with the same transition frequency, unless they accidentally fall very close to the shifted potential's threshold. Thus the $\langle \phi_f | r | \phi_i \rangle$ are about equal, except that states in the continuum are energy-normalized. This produces a density of states factor,

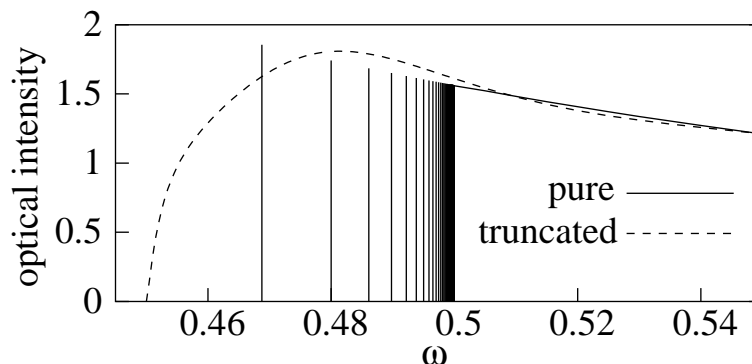


Figure 3.2: Oscillator strengths (in inverse Hartrees) corresponding to $1s \rightarrow np$ transitions (only shown for $n \geq 4$) for a pure Coulomb and the truncated-Coulomb potential given by Eq. (3.3) with $1/C = 20$.

$(dE/dn)^{-1}$, where n is the final state index. In the case of a pure $-1/r$ potential, this is simply n^3 . Once this is accounted for, the optical response of the truncated potential is very close to that of the long-ranged potential.

3.1.2 LDA potentials

Why is this phenomenon relevant to a TDLDA optical spectrum? Long ago, it was understood that the primary difference between LDA (or GGA) potentials and the exact KS potential is due to a lack of derivative discontinuity in the LDA potential [68]. This leads to the LDA XC potential differing from the exact XC potential by (nearly) a constant in the valence region: about $(I + A)/2$ where I is the ionization potential and A the electron affinity. Taking $I = 0.8$ and $A \approx 0$ yields a shift of 0.4 as shown in Fig.3. The variation of the difference with r is much smaller than that of the potentials in the valence region of the Ne atom.

To plot the Rydberg series of an exact KS potential, we write $E_{nl} = -(n - \mu_{nl})^{-2}/2$, where μ_{nl} is the quantum defect, typically a very smooth function of n , and rapidly approaching a finite value as $n \rightarrow \infty$. To interpolate the n -dependence of μ , we used the same self-consistent interpolation of Al-Sharif et.

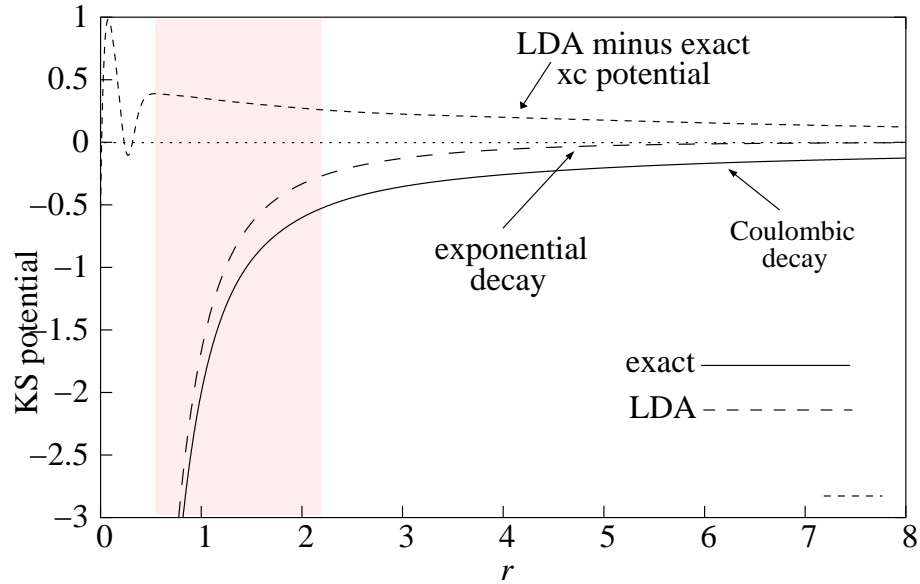


Figure 3.3: Ne atom: the top curve shows the difference between the LDA and exact XC-potential. The bottom curves show v_s^{exact} and v_s^{LDA} . In the valence region (shaded) the two potentials run almost parallel.

al. [46]. In practice, $(dE/dn)^{-1}$ differs negligibly from $(n - \mu_{nl})^3$ [43].

In Fig.(3.1), we plot the KS optical response spectrum for the Ne atom, for both the LDA and exact potentials. The LDA potential was obtained through a fully numerical self-consistent calculation [69]. The high quality of the LDA spectrum is already apparent in the bare KS spectrum (in the case of the Ne atom, the TDDFT corrections are small[32]). The LDA threshold is 0.3 (8eV) below the exact threshold. Above the LDA threshold, the LDA oscillator strength is accurate to within 20% for all bound transitions. Table I shows this explicitly by extracting these from the height of the LDA curve at the exact transition frequencies. These LDA states are not resonances, but simple continuum states. From the table we see that LDA is accurate, even if not as accurate as OEP (the error from the latter is largely due to lack of correlation in the HOMO [70]). Thus, while not yielding directly an approximation to the eigenvalues (although see Sec.3.2), accurate oscillator strengths are available from LDA (or GGA) if the

Table 3.1: Oscillator strengths for the first six discrete $2p \rightarrow ns$ transitions in Ne.[LDA numbers extracted from the height of the LDA continuum curve at the exact transition frequencies].

Transition	LDA	OEP	exact
2p \rightarrow 3s	2.22(-2)	2.84(-2)	2.70(-2)
2p \rightarrow 4s	3.74(-3)	4.43(-3)	4.46(-3)
2p \rightarrow 5s	1.32(-3)	1.54(-3)	1.57(-3)
2p \rightarrow 6s	6.22(-4)	7.15(-4)	7.34(-4)
2p \rightarrow 7s	3.42(-4)	3.91(-4)	4.03(-4)
2p \rightarrow 8s	2.09(-4)	2.37(-4)	2.45(-4)

exact transition frequencies are known.

The Thomas-Reiche-Kuhn sum rule states that the total oscillator strength integrated over all frequencies is proportional to N , the number of electrons [43]:

$$\sum_n F_{ni} + \int_I^\infty dE \frac{dF_{Ei}}{dE} = 3N \quad . \quad (3.5)$$

We verified the satisfaction of Eq.(3.5) in all our calculations. It is interesting to see how the total optical intensity accumulates as a function of frequency. The bottom panel of Fig.(3.4) shows this for the coulomb and truncated coulomb potentials, when $r_0 = 20$. In between the two ionization thresholds (the coulomb threshold I and the truncated-coulomb threshold I_{tr}), the total optical intensity of the truncated-coulomb potential accumulates in a smooth way in such a way that at the threshold I the frequency-integrated oscillator strength is close to that of the pure coulomb potential, accumulated in a step-wise fashion. Similar curves are observed in the case of Ne for the LDA vs. the exact KS potential, Fig.(3.5).

But the accuracy of the LDA spectrum is *not* simply a consequence of the TRK sum rule. After all, any one-body potential satisfies this. Rather, it is the detailed shape of the LDA KS-potential that is important. LDA densities are close to exact densities, implying that occupied orbitals are quite accurate. In particular, the LDA HOMO (2p in this case), out of which we are computing the transitions, is almost identical to the exact HOMO (Fig.(3.6)). This fact alone

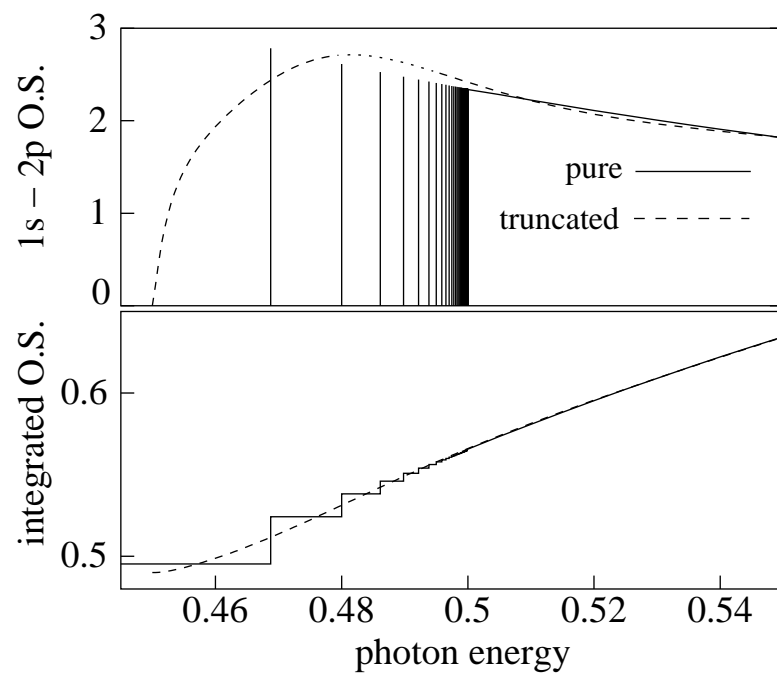


Figure 3.4: Bottom panel: Integrated oscillator strength as a function of frequency for the pure and truncated coulomb potentials; $r_0 = 20$ in this plot.

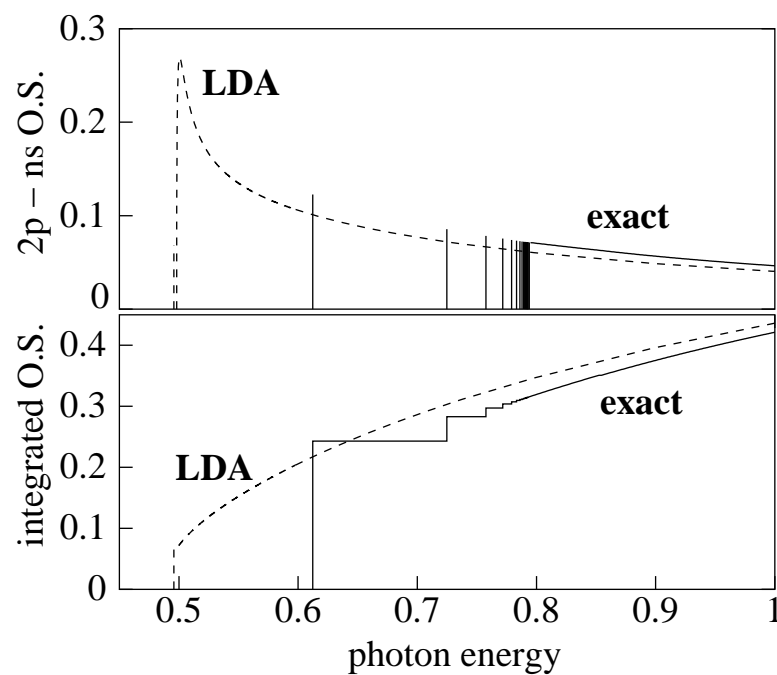


Figure 3.5: Bottom panel: Integrated oscillator strength as a function of frequency for the exact and LDA potential of the Ne atom

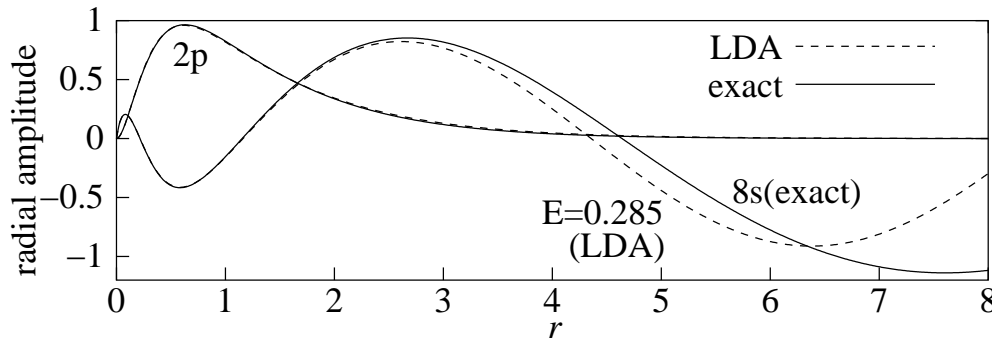


Figure 3.6: Ne atom: LDA *continuum* state at energy $E=0.2853$, and exact energy-normalized $8s$ *bound* orbital, along with the LDA and exact $2p$ orbitals.

implies accurate behavior for the high frequency limit of the optical spectrum. To see this, evaluate the dipole matrix element assuming the final state is a simple plane wave, as it will be when its energy is very high. One finds that (see Appendix F):

$$\int_0^\infty dr \phi_{np}(r) r \phi_{\epsilon, l=0} \xrightarrow{\epsilon \rightarrow \infty} -\frac{3Z}{2^{5/4} \sqrt{\pi}} \phi_{np}''(r=0) \epsilon^{-11/4} \quad (3.6)$$

where Z is the nuclear charge. Thus an accurate HOMO near the nucleus yields accurate high-frequency behavior. Even at frequencies only slightly below the exact threshold, the final states are similar in regions that are significant for the optical response, and their different asymptotic behavior is irrelevant, as shown in Fig.(3.6).

We now discuss where the LDA response will *not* be accurate, namely in the immediate vicinity of the LDA threshold. At this threshold, the LDA response incorrectly vanishes according to Wigner-threshold behavior [71]. How far above this value must one be to trust the accuracy of the LDA spectrum? To see this, we again truncate the Coulomb potential of Fig.(3.2) (where the truncation point was chosen appropriately for comparison purposes) but now choose a range of truncation values, $r_0 = 20 \rightarrow 10$, so that the threshold of the truncated spectrum, I_{tr} , *passes through* a discrete transition of the exact potential. Fig.(3.7)

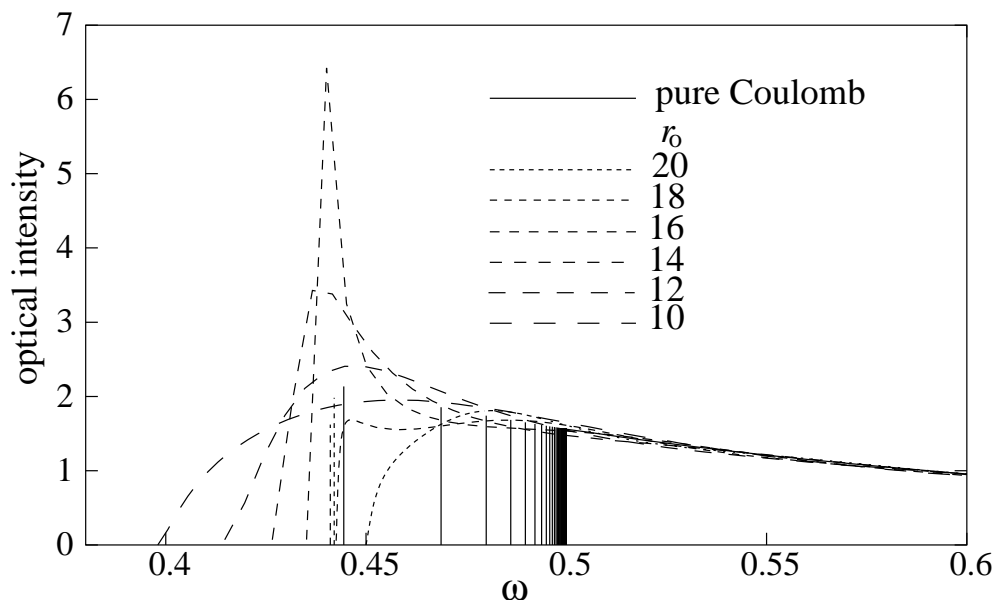


Figure 3.7: The threshold of the truncated spectrum passes through the $1s \rightarrow 3p$ discrete transition of the pure Coulomb potential as r_0 goes from 18 to 16.

shows that, as a discrete transition is absorbed into the continuum, its oscillator strength is at first a sharp peak centered on I_{tr} . When I_{tr} is well-below the discrete transition, this peak has settled to an accurate envelope for that transition. Thus one can trust the truncated oscillator strength for all discrete transitions absorbed in the continuum except possibly the lowest. *Only* very close (within one transition on either side) to I_{tr} is the truncated spectrum inaccurate. In the case of Ne in Fig.(3.1), there is a barely bound transition (energy -2.3mH) in the LDA spectrum, whose oscillator strength has been partially absorbed by the continuum.

In Fig.(3.8) we plot the $2p \rightarrow nd$ transitions for Ne and observe again that the LDA does a very good job, even near threshold. Finally, Fig.(3.9) shows both the bare KS response and the TDDFT corrected response of the He atom; the latter both exactly (from experiment and accurate quantum chemical calculations) and within TDLDA. These are the results of Stener et al. [72], but we do not shift the LDA spectrum to correct for the threshold error: we compare

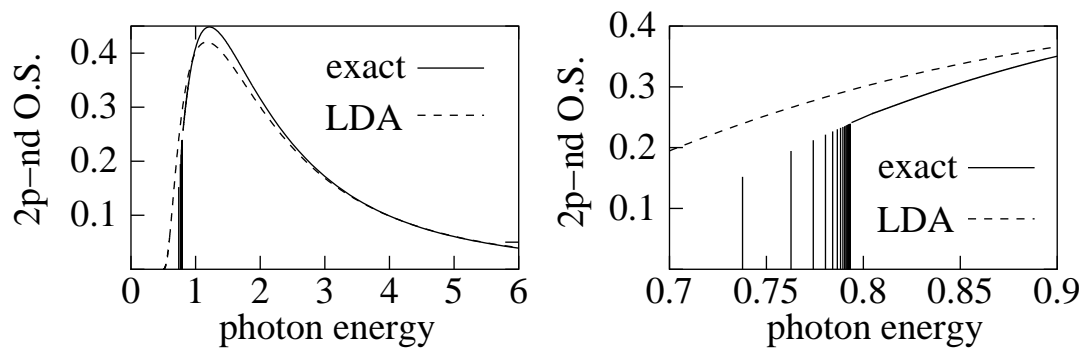


Figure 3.8: $2p \rightarrow nd$ spectrum of Ne, plotted as in Fig. 1. as a function of photon energy, from the exact KS potential, and from the LDA one.

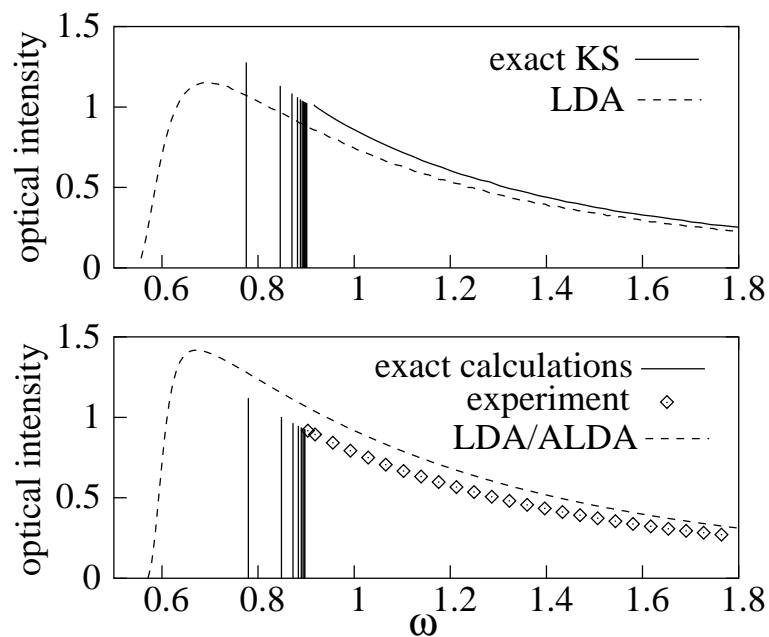


Figure 3.9: He atom: The top panel shows the bare exact KS and LDA spectra, and the lower panel shows the TDDFT corrected spectra, LDA/ALDA results are from [72] but unshifted; the exact calculations are from [73], multiplied by the density of states factor (see text), and the experimental results are from [74].

oscillator strengths at the same frequency, not energy. The TDDFT corrections are small, and overcorrect the bare LDA results, but clearly are consistent with our observations for the bare spectra.

Often the excited state *energy* is of primary interest, especially to quantum chemists focussed on molecular spectroscopy. However, for many other properties, the integrated response is relevant. The dispersion forces between separated molecules are determined by the (imaginary) frequency integral of the dynamic polarizabilities of the individual species. Our results imply that even LDA should be an excellent approximation, as was found in Ref. [75], and more recently in Ref. [76] for finite distances.

Moreover, it can happen that a bound \rightarrow bound transition is shifted into the continuum by TDLDA, but if it remains strongly peaked, our analysis shows that the transition frequency and photoabsorption intensity for this transition can be trusted, even though the transition is now bound \rightarrow free. The $\pi \rightarrow \pi^*$ transition in benzene is an example of this [64]. In summary: this is one of those rare cases where the results of an approximation are qualitatively wrong, but quantitatively accurate. It has been argued that LDA yields inaccurate atomic photoionization cross-sections within TDDFT, and that transitions to Rydberg states cannot be studied within LDA. On the contrary, LDA gives accurate optical spectra of atoms and molecules when interpreted appropriately. We also note that, for those interested in the $\omega > 0$ spectrum, TDLDA should be trusted, not shifted.

3.2 Rydberg excitation energies from LDA scattering states

So far we have shown [77] that in spite of incorrectly describing photoabsorption as if it were photoionization, the oscillator strengths of Rydberg excitations show up in the LDA spectrum as continuum contributions with excellent optical intensity. The dipole matrix elements for HOMO \rightarrow Rydberg transitions are accurate in

LDA because (1) the shape of the LDA HOMO is very close to that of the exact KS HOMO, even if its energy is not, and (2) LDA continuum orbitals at frequencies corresponding to HOMO \rightarrow Rydberg transitions, are also very close to the exact KS Rydberg orbitals in the crucial region for optical absorption, i.e. where the HOMO has high amplitude. The underlying physical reason for this is simple: the LDA exchange-correlation potential is a good approximation to the exact XC potential near the nuclei, and runs almost parallel to it in the valence regions [77], [78].

A possible objection to this claim of success of the LDA is that it cannot predict the *positions* of the Rydberg excitations, even if it produces an ionization envelope that approximates well the discrete photoabsorption spectrum. We now show that, in fact, LDA *can* predict the position of high- n Rydberg excitations very accurately. We use concepts of quantum defect theory, developed before the advent of DFT by Ham [79] and Seaton [47]. The quantum defect μ_{nl} parametrizes the energy E_{nl} of a Rydberg state as in Eq.(2.32):

$$E_{nl} = -\frac{1}{2(n - \mu_{nl})^2} . \quad (3.7)$$

For an electron orbiting in a Coulomb field outside an ionic core, as in a high- n Rydberg state, μ_{nl} represents the effect of the field that prevails *within* the core. Even though the Coulomb field outside the core is invoked for its definition in Eq.(3.7), the actual number μ_{nl} is determined only by the forces inside the core [80]. It is typically a very smooth function of n , and approaches rapidly a finite value as $n \rightarrow \infty$, the asymptotic quantum defect, μ_l .

We will focus on the KS asymptotic quantum defect of the ($l = 0$)-Rydberg series that converges to the first ionization threshold of an atom. In Subsection 3.2.1 we propose a method to extract μ from the orbitals. In Subsection 3.2.2 we test the method in two simple examples, and in Subsection 3.2.3 we apply it to the cases of He and Ne, where the exact KS quantum defects are known, and show that the LDA produces μ 's which are in less than 5% error.

3.2.1 Quantum defect from its orbital

Consider a potential that equals $-1/r$ for $r \geq r_0$. The solution of the radial Schrödinger equation is well known for $r \geq r_0$. For negative energies $E < 0$, the physically acceptable solutions are Whittaker functions (we will restrict the analysis to s -states):

$$\phi_{>r_0}(r) = AW_{1/k, 1/2}(2kr) \quad , \quad (3.8)$$

where A is a constant and $k = \sqrt{2|E|}$. The logarithmic derivative of $\phi_{>r_0}$ is given by:

$$\frac{d \ln \phi_{>r_0}}{dr} = \frac{1}{n^*} - \frac{n^*}{r} - \frac{1}{r} \frac{U(-n^*; 2; 2r/n^*)}{U(1-n^*; 2; 2r/n^*)} \quad (3.9)$$

Here k was written as $k = (n^*)^{-1}$, with $n^* = (n - \mu_n)$, where n numbers the bound state, and μ_n is the quantum defect; U is the U -confluent hypergeometric function [81].

Regardless of the shape of the potential for $r < r_0$, the logarithmic derivative of $\phi_{<r_0}$ must equal that of $\phi_{>r_0}$ at r_0 . Now suppose that an orbital is given to us, with the information that it is the $n = 8$ state of a potential that possesses a Coulomb tail. We can immediately obtain μ from this orbital by solving Eq.(3.9) numerically, using $n = 8$ and some large value of r . If we observe that μ changes as r is increased, we can conclude that Eq.(3.9) is being used in the region where $r < r_0$, and its solution can not be interpreted as the quantum defect.

3.2.2 Two examples

Potential with constant core and Coulomb tail

Consider a potential which is equal to a constant C for $r < r_0$ and to $-1/r$ for $r \geq r_0$. For $r_0 = 1$ the matching condition is:

$$\tilde{k} \coth \tilde{k} = \frac{1}{n^*} - n^* - \frac{U(-n^*; 2; 2/n^*)}{U(1-n^*; 2; 2/n^*)} \quad (3.10)$$

where $\tilde{k} = \sqrt{2|E - C|}$. Eq.(3.10) was solved for the first 20 bound states. For $C = r_0 = 1$ the asymptotic quantum defect is $\mu = -0.441$, see Fig.(3.10). Figure (3.11) shows $\mu(r)$, the solution of Eq.(3.9) as a function of r , for the $n = 20$ orbital. Clearly, the quantum defect for a given state can be obtained by looking at the respective orbital anywhere in the region $r > r_0$. In particular, it can be obtained *at* r_0 . It represents the accumulation of phase due to the non-coulombic potential in the region of $r < r_0$ up to $r = r_0$.

Imagine now that the potential is altered by replacing the Coulomb tail by an exponential decay. This modified potential has an orbital which –up to a constant– is identical to the original $n = 20$ Rydberg orbital in the region $r < r_0$, but it is now a *scattering* orbital, behaving very differently in the region $r > r_0$. We can *still* solve Eq.(3.9) on this scattering orbital, with $n = 20$ on the right-hand side, and find $\mu = -0.441$ at r_0 . The altered potential does not have a Rydberg series, yet the solution of Eq.(3.9) at r_0 can still be interpreted as the asymptotic quantum defect of the Rydberg series that was lost as a consequence of the alteration.

The Coulomb tail has nothing to do with the *value* of μ . It only has to do with its definition.

Potential that yields $\mu = 1$

Take $\phi_{>r_0}$ to be the 7th Coulomb Rydberg orbital, meant to represent (for $r > r_0$) the 8th orbital of some potential which differs from $-1/r$ for $r < r_0$, but equals $-1/r$ for $r \geq r_0$. Applying Eq.(3.9) for any $r > r_0$ we find correctly $\mu = 1$, because $n = 8$ in the right-hand-side of Eq.(3.9). One of the nodes has been shifted into the region $r < r_0$.

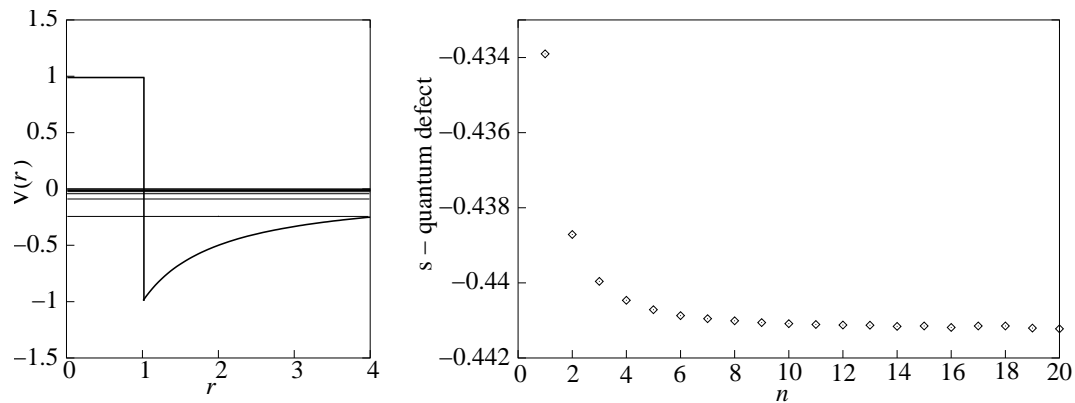


Figure 3.10: *Left*: Potential with constant core ($C = 1$) and Coulomb tail beginning at $r_0 = 1$. Its energy spectrum is indicated by horizontal lines. *Right*: s -quantum defect as a function of n for the potential of the first example. The quantum defect is a smooth function of n and converges rapidly to its asymptotic value, $\mu = -0.441$.

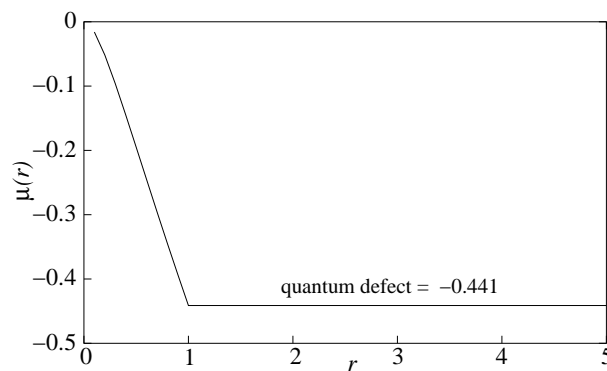


Figure 3.11: Solution of Eq.(3.9) for μ as a function of r , for the potential of the first example; the logarithmic derivative of the $n = 20$ orbital was found numerically as a function of r , and at each location r , it was inserted into Eq.(3.9) to get $\mu(r)$

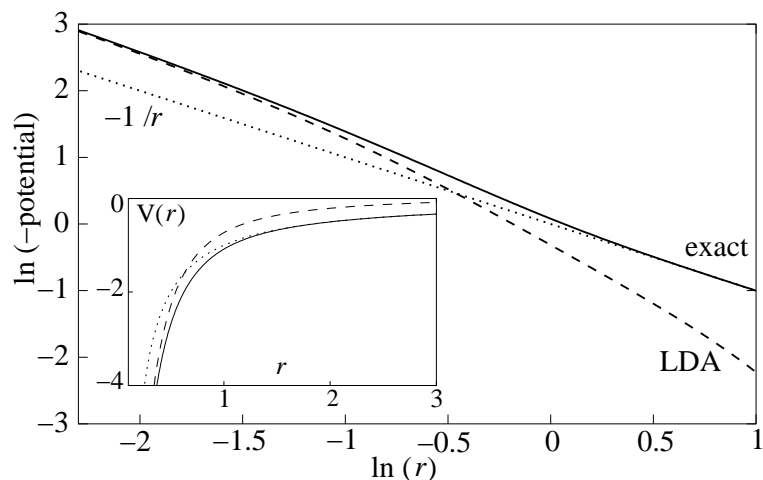


Figure 3.12: Comparison of the exact KS potential of the He atom [48] (solid line), and the LDA potential (dashed line). The Coulomb potential is also shown (dotted line). At $r \sim 1$ the exact potential is almost Coulombic. The inset shows the potentials themselves.

3.2.3 Results for Helium and Neon

Helium

Consider the first s -Rydberg series of the He atom. Fig.(3.13) shows the s -quantum defect as a function of n from the *exact* KS potential obtained by Umrigar and Gonze [48]. The asymptotic quantum defect $\mu = 0.213$ can be extracted through Eq.(3.9) from e.g. the $n = 20$ orbital, just as it was done in the first example of the last Section. It is clear from Fig.(3.14) that at $r_0 \sim 1$, Eq.(3.9) is already giving an accurate value of μ . This is a remarkable fact, not at all obvious considering that the KS potential at $r \sim 1$ is still not equal to $-1/r$ (see Fig.3.12). Most of the quantum defect is built up close to the nucleus (step rise for $0 < r < 1$ in Fig.(3.14)), and its final value of $\mu \sim 0.213$ has been reached before the potential becomes purely coulombic.

The LDA potential runs almost parallel to the exact one in the region $1 < r < 2$ (where μ can already be extracted accurately), and orbitals corresponding to the same *frequency* (exact and LDA) are therefore very close in that region,

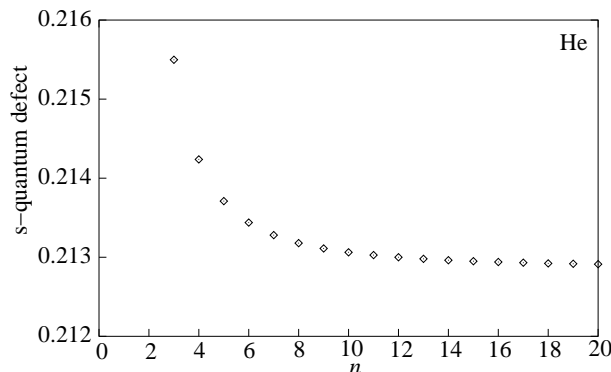


Figure 3.13: s -quantum defect as a function of n for the exact KS potential [48] of the He atom. The quantum defect converges rapidly to its asymptotic value, $\mu = 0.213$.

see Fig.(3.15). In the spirit of ref.[77], we compare the exact 20s orbital (which is essentially identical to the zero-energy state in the region $0 < r < 6$) and the LDA orbital of energy $I + \epsilon_{1s}^{LDA} = 0.904 - 0.571 = 0.333$. Notice how good the LDA orbital is in the region $1 < r < 2$. We show in Fig.(3.16) the solution of Eq.(3.9) when this scattering LDA orbital is employed. Clearly, the plateau of the LDA curve in the $1 < r < 2$ region is an accurate estimate of the quantum defect. The value of μ on this plateau is 0.205, an underestimation of less than 4% with respect to the exact value. Thus, given the true ionization potential of the system, LDA gives a very accurate prediction of the asymptotic quantum defect.

Neon

We repeat the same for the Ne atom. This time we choose the $n = 8$ state, whose corresponding LDA energy is $E = 0.285$. The first plateau of the LDA curve in Fig.(3.17) is at $\mu = 1.366$, an overestimation of 4% with respect to the exact value ($\mu = 1.313$). We can now construct a purely LDA spectrum with Rydberg excitations, Table 3.2 and Fig.(3.18).

It may be argued that our approach is equivalent to asymptotically correcting

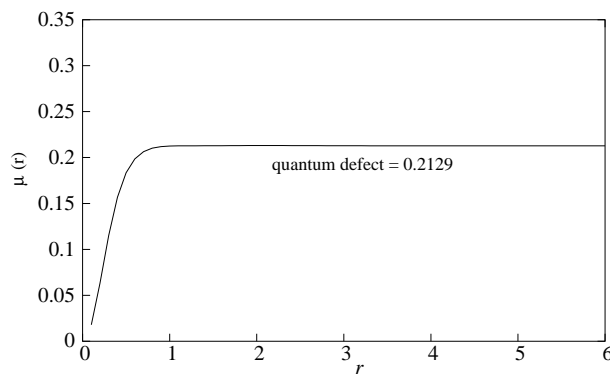


Figure 3.14: He atom: solution of Eq.(3.9) for μ as a function of r ; The $n = 20$ orbital was used

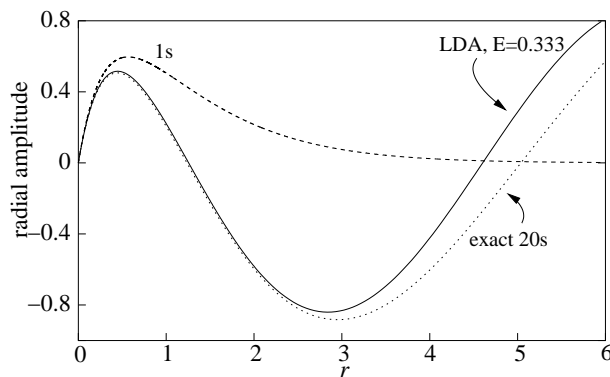


Figure 3.15: Radial orbitals of He: LDA orbital of energy $E=0.333$ and exact 20s orbital; the HOMO is also shown. Notice that the LDA scattering orbital and the exact KS Rydberg orbital are very close in the region $1 < r < 2$, where the quantum defect can be extracted (see text, and Fig.3.16). The fact that the LDA orbital has an incorrect asymptotic behavior at large r is irrelevant for the value of μ , as well as for optical absorption [77]

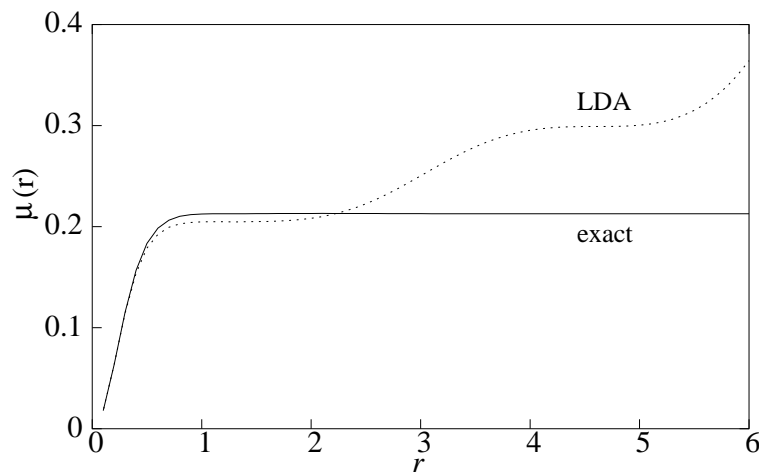


Figure 3.16: He atom: solution of Eq.(3.9) for μ as a function of r ; The $n = 20$ orbital was used for the exact case, and the $E=0.333$ orbital was used for the LDA (the value of n in Eq.(3.9) was set large enough in this case to ensure convergence)

Table 3.2: Transition frequencies and oscillator strengths in atomic units for the first six discrete $2p \rightarrow ns$ transitions in Ne, from the exact and LDA KS potentials.

trans.	transition frequency		oscillator strength	
	LDA	exact	LDA	exact
2p→3s	0.6052	0.6102	2.38(-2)	2.70(-2)
2p→4s	0.7204	0.7227	3.99(-3)	4.46(-3)
2p→5s	0.7546	0.7556	1.39(-3)	1.57(-3)
2p→6s	0.7692	0.7697	6.49(-4)	7.34(-4)
2p→7s	0.7767	0.7770	3.55(-4)	4.03(-4)
2p→8s	0.7811	0.7813	2.15(-4)	2.45(-4)

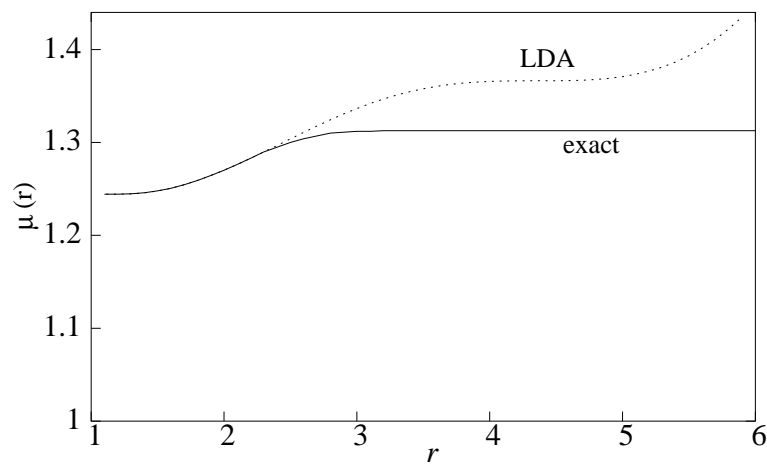


Figure 3.17: Ne atom: solution of Eq.(3.9) for μ as a function of r ; The $n = 8$ orbital was used for the exact case, and the $E=0.285$ orbital was used for the LDA.

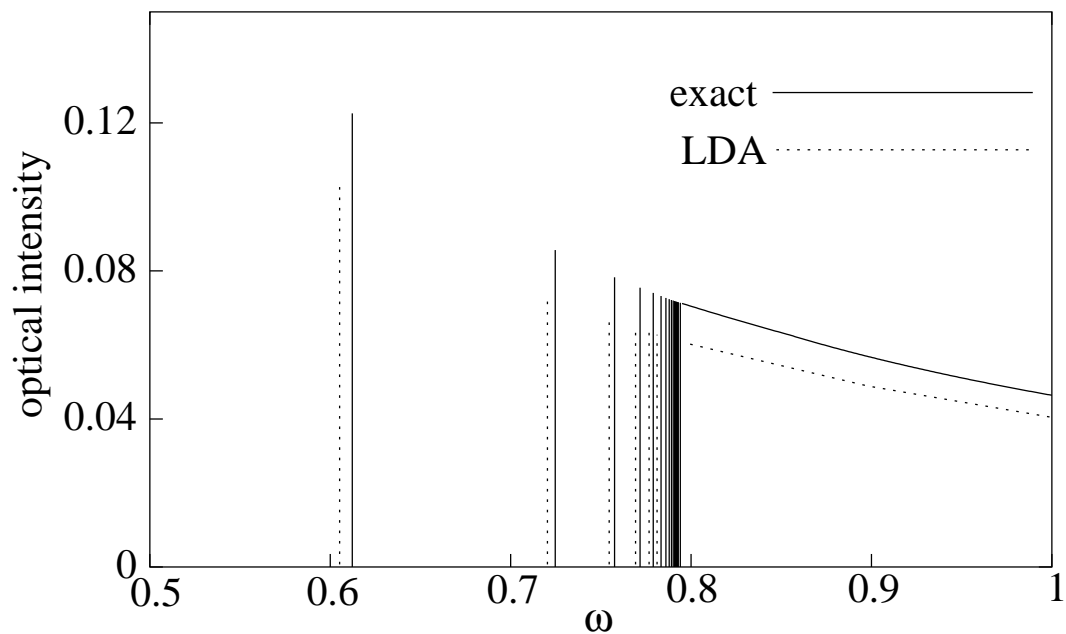


Figure 3.18: Ne atom: Like in Fig.(3.1), but now using the LDA excitation energies as listed in Table 3.2.

the LDA potential, e.g., à la van Leeuwen-Baerends [56]. Calculations should be done to address this point and compare the two approaches. Our non-invasive method leaves the LDA potential intact: instead of modifying the shape of the potential, we modify the interpretation of the results of a *pure* DFT-LDA calculation. No spurious effects due to shifting-and-splicing the potentials [57] appear.

We have shown that, given the experimental ionization potential of an atom, an LDA calculation yields an accurate value for the asymptotic quantum defect of the Rydberg series converging to that threshold. Through Seaton's theorem [47] ($\pi\mu = \delta(E \rightarrow 0^+)$), this also implies that LDA yields accurate low-energy phase shifts for an electron scattering from the corresponding positive ion; work along this line is ongoing. We have not addressed here the effect of dynamical corrections to the quantum defects; work along this line is also ongoing. Can the method presented here be extended to get LDA predictions for low- n states? We believe so, and work along this line is ongoing too.

Appendix A

Extracting transmission amplitudes from the susceptibility in 1d

A.1 Derivation of Eq.(2.11)

Let's study the integral of Eq.(2.9),

$$J = \int_{0[\text{R}],[\text{L}]}^{\infty} \frac{\phi_k(x)\phi_k^*(x')}{\omega - \Omega_k + i\eta} dk, \quad (\text{A.1})$$

in the limit when $x \rightarrow -\infty$ and $x' \rightarrow -x$. The one-electron orbital $\phi_k(x)$ has the scattering boundary conditions indicated by Eq.(2.10), so that

$$J \xrightarrow[\substack{x \rightarrow -\infty \\ x' \rightarrow -x}]{} \int_0^{\infty} dk \frac{(e^{ikx} + r_k e^{-ikx}) t_k^* e^{ikx}}{\omega - k^2/2 - I + i\eta} + \int_0^{\infty} dk \frac{(e^{-ikx} + r_k^* e^{ikx}) t_k e^{-ikx}}{\omega - k^2/2 - I + i\eta}, \quad (\text{A.2})$$

where the first term corresponds to [R], and the second to [L]-boundary conditions. I is the ionization energy of the $(N + 1)$ -electron system, and k the wavenumber of the projectile electron. Using the following properties of the transmission and reflection amplitudes:

$$t_k^* = t_{-k}, \quad r_k^* = r_{-k}, \quad (\text{A.3})$$

Eq.(A.2) can be rewritten as:

$$J \xrightarrow[\substack{x \rightarrow -\infty \\ x' \rightarrow -x}]{} \int_{-\infty}^{+\infty} dk \frac{t_k e^{-2ikx}}{\omega - k^2/2 - I + i\eta} + \int_{-\infty}^{+\infty} dk \frac{r_k^* t_k}{\omega - k^2/2 - I + i\eta} \quad (\text{A.4})$$

With all the poles of t_k lying on the positive imaginary k -axis, the first of these terms yields:

$$\int_{-\infty}^{+\infty} dk \frac{t_k e^{-2ikx}}{\omega - k^2/2 - I + i\eta} = -\frac{2\pi i}{\tilde{k}} t_{\tilde{k}} e^{-2i\tilde{k}x} - 4\pi i \mathcal{R}(\text{poles of } t_k), \quad \tilde{k} = \sqrt{2(\omega - I)}, \quad (\text{A.5})$$

where the residues \mathcal{R} (poles of t_k) decay exponentially at large distances.

According to Eq.(2.8), the complex-conjugate of J when $\omega \rightarrow -\omega$ also needs to be considered, but inspection of Eq.(A.2) shows that this term will only contribute with exponentially decaying terms at large distances.

With Eqs.(A.4) and (A.5) into Eqs.(2.8) and (2.9), the susceptibility at large distances is:

$$\chi(x, -x; \omega) \xrightarrow{x \rightarrow -\infty} -\frac{i}{\tilde{k}} \sqrt{\rho(x)\rho(-x)} t_{\tilde{k}} e^{-2i\tilde{k}x} \delta_{0,n_t} \delta_{S_0,S_n} + \text{n.o.} , \quad (\text{A.6})$$

where ‘‘n.o.’’ stands for non-oscillatory terms. Denoting by χ^{osc} the oscillatory part of χ (the coefficient of $\exp[-2i\tilde{k}x]$), the transmission amplitude at energy ε for elastic ($\delta_{0,n_t} = 1$), spin-conserving ($\delta_{S_0,S_n} = 1$) collisions, is given by Eq.(2.11):

$$t(\varepsilon) = \lim_{x \rightarrow -\infty} \left[\frac{i\sqrt{2\varepsilon}}{\sqrt{\rho(x)\rho(-x)}} \chi^{\text{osc}}(x, -x; \varepsilon + I) \right] . \quad (\text{A.7})$$

A.2 Derivation of Eq.(2.12)

The same steps of the previous section apply to non-interacting electrons, so Eq.(2.12) has exactly the same form as Eq.(2.11): the Kohn-Sham transmission amplitudes can be extracted from the Kohn-Sham susceptibility just as the true amplitudes of the interacting system are extracted from the (true, interacting) susceptibility. For non-interacting electrons, however, we also give an alternative derivation of Eq.(2.12), starting from the following representation of the Kohn-Sham susceptibility:

$$\chi_s(x, x'; \omega) = \sum_{occ} \phi_i(x) \phi_i(x') g_s(x, x'; \omega + \epsilon_i) + c.c.(\omega \rightarrow -\omega) , \quad (\text{A.8})$$

with

$$g_s(x, x'; \varepsilon) = -\frac{2}{W} \phi_L(x_<) \phi_R(x_>) , \quad (\text{A.9})$$

where the wronskian $W = \phi_R \phi'_L - \phi_L \phi'_R$ is taken for Kohn-Sham orbitals ϕ_R and ϕ_L satisfying right and left boundary conditions respectively, as in Eq.(2.10). W

is independent of position; evaluating it as $x \rightarrow \infty$ we get $W = -2ikt_k$, where k is the wavenumber corresponding to ε . Since the ϵ_i 's are all negative (the index i in Eq.(A.8) runs over the $N + 1$ *occupied* KS orbitals), the complex conjugate term in Eq.(A.8) is not oscillatory, and decays at large distances. The HOMO is the less rapidly decaying KS orbital, going as the square root of the density at large distances, and $\epsilon_{\text{HOMO}} = -I$, so Eqs.(A.9) and (A.8) yield:

$$\begin{aligned} \chi_s(x, x'; \omega) &\xrightarrow[\substack{x \rightarrow -\infty \\ x' \rightarrow -x}]{} \phi_{\text{HOMO}}(x)\phi_{\text{HOMO}}(-x)g_s(x, x'; \omega - I) & \text{(A.10)} \\ &= \sqrt{\rho(x)\rho(-x)} \frac{1}{i\tilde{k}t_{\tilde{k}}} \left(t_{\tilde{k}}e^{-i\tilde{k}x}\right)^2, \quad \tilde{k} = \sqrt{2(\omega - I)} \end{aligned} \quad \text{(A.11)}$$

leading directly to Eq.(2.12). Notice that no non-oscillatory terms – like the second term of Eq.(A.4) – appear in this derivation (apart from those that are exponentially small at large distances).

Appendix B

Elastic scattering in 1d

B.1 Parity-wave analysis of 1d-scattering

We call it “parity-wave” in analogy to the usual “partial-wave” analysis of 3d-scattering, as suggested by Eberly [82]. For Schrödinger’s equation in 1d:

$$\left(-\frac{1}{2}\frac{d^2}{dx^2} + v(x) - \frac{k^2}{2}\right)\psi(x) = 0 \quad , \quad (\text{B.1})$$

write the solution at large distances as:

$$\psi_k(r) \xrightarrow{r \rightarrow \infty} e^{ikr\epsilon} + f(\epsilon)e^{ikr} \quad (\text{B.2})$$

where $r = |x|$, and $\epsilon = \text{sign}(x)$. Comparing with Eq.(2.10) one concludes that:

$$t_k = 1 + f(+), \quad r_k = f(-) \quad . \quad (\text{B.3})$$

Calculation of the current yields:

$$j(\epsilon) = \frac{i\epsilon}{2} \left(\frac{\partial\psi^*}{\partial r}\psi - \psi^*\frac{\partial\psi}{\partial r} \right) \quad (\text{B.4})$$

$$\xrightarrow{r \rightarrow \infty} k \left[1 + \epsilon|f(\epsilon)|^2 + \Re \left\{ (1 + \epsilon)f(\epsilon)e^{ik(1-\epsilon)r} \right\} \right] \quad . \quad (\text{B.5})$$

Conservation of probability $j(+)=j(-)$ leads to the optical theorem:

$$\sigma = -2\Re f(+), \quad (\text{B.6})$$

where the total cross section σ is the sum of two ‘differential’ cross-sections:

$$\sigma = \sum_{\epsilon} \sigma(\epsilon), \quad \sigma(\epsilon) = |f(\epsilon)|^2 \quad . \quad (\text{B.7})$$

B.2 Phase shifts

Still following Eberly [82], it is possible to write $\psi(r \rightarrow \infty)$ as a sum of even and odd parity waves:

$$\psi(r) \xrightarrow{\infty} \sum_{l=0}^1 \epsilon^l A_l \cos(kr + l\pi/2 + \delta_l) \quad (\text{B.8})$$

Now expand $f(\epsilon)$ as:

$$f(\epsilon) = \sum_{l=0}^1 \epsilon^l f_l \quad , \quad (\text{B.9})$$

and write the asymptotic wavefunction (B.2) as

$$\psi(r) \xrightarrow{r \rightarrow \infty} \cos kr + f_0 e^{ikr} + \epsilon(i \sin kr + f_1 e^{ikr}) \quad . \quad (\text{B.10})$$

Comparing Eqs.(B.8) and (B.10), and matching coefficients of e^{-ikr} and e^{ikr} for each parity wave, we conclude that

$$A_l = (-i)^l e^{i\delta_l} \quad , \quad f_l = i e^{i\delta_l} \sin \delta_l \quad . \quad (\text{B.11})$$

Inserting Eq.(B.11) into Eq.(B.7):

$$f(\epsilon) = i \sum_{l=0}^1 \epsilon^l e^{i\delta_l} \sin \delta_l \quad . \quad (\text{B.12})$$

B.2.1 Particular cases

Delta function: If $v(x) = Z\delta(x)$ then [83]:

$$\delta_0 = \tan^{-1} \left(-\frac{Z}{2k} \right) \quad , \quad (\text{B.13})$$

$$\delta_1 = 0 \quad . \quad (\text{B.14})$$

Square barrier: If $v(x) = 0$ for $r > a$ and $v(x) = -V_0$ for $r \leq a$ then [82]:

$$\delta_0 = \tan^{-1} \left(\frac{\kappa}{k} \tan \kappa a \right) - ka \quad , \quad (\text{B.15})$$

$$\delta_1 = \tan^{-1} \left(\frac{k}{\kappa} \tan \kappa a \right) - ka \quad , \quad (\text{B.16})$$

where $\kappa^2 = k^2 + 2V_0$.

B.3 Transmission amplitude from Lippmann-Schwinger's equation

The 1d-Lippmann Schwinger equation is [83]:

$$\psi_k(x) = \phi_k(x) + \int_{-\infty}^{\infty} g_0(x, x') v(x') \psi_k(x') dx' \quad , \quad (\text{B.17})$$

where the incident plane wave $\phi_k(x) = \exp(ikx)$ satisfies Eq.(B.1) with $v(x) = 0$.

Introducing the free-particle Green function

$$g_0(x, x') = \frac{1}{ik} e^{ik|x-x'|} \quad (\text{B.18})$$

into Eq.(B.17), taking the limit $r \rightarrow \infty$, and comparing with Eqs.(B.2) and (B.3), one gets the following expression for the transmission amplitude:

$$t_k = 1 + \frac{1}{ik} \int_{-\infty}^{\infty} dx e^{-ikx} v(x) \psi_k(x) \quad (\text{B.19})$$

B.4 Born approximation in TDDFT

In the limit $x \rightarrow \infty$, Eq.(A.8) for the KS susceptibility $\chi_s(x, x'; \omega)$ yields:

$$\chi_s(x, x'; \omega) = \sum_{i \text{ occ}} \phi_{s,i}^*(x) \phi_{s,i}(x') g_s(x, x'; \epsilon_i + \omega) + c.c. (\omega \rightarrow -\omega) \quad (\text{B.20})$$

$$\xrightarrow{x \rightarrow \infty} \sqrt{\rho(x)} \phi_{sH}(x') g_s(x, x'; \omega - I) \quad , \quad (\text{B.21})$$

where ϕ_{sH} is the KS HOMO. The asymptotic behavior of the KS Green function, Eq.(A.9) is:

$$g_s(x, x'; \varepsilon) \xrightarrow{x \rightarrow \infty} \frac{1}{ik} \phi_{sk}^{[L]}(x') e^{ikx} \quad (\text{B.22})$$

$$\xrightarrow{x > x' \rightarrow \infty} \frac{1}{ik} \left[e^{-ikx'} + r_s e^{ikx'} \right] \quad , \quad (\text{B.23})$$

implying from Eq.(B.21) that:

$$\chi_s(x, x'; \omega) \xrightarrow{x \rightarrow \infty} \frac{\sqrt{\rho(x)}}{ik} \phi_{sH}(x') \phi_{sk}^{[L]}(x') e^{ikx} \quad (\text{B.24})$$

$$\xrightarrow{x > x' \rightarrow \infty} \frac{\sqrt{\rho(x)\rho(x')}}{ik} e^{ikx} \left[e^{-ikx'} + r_s e^{ikx'} \right] \quad (\text{B.25})$$

Now define the function $\phi_{\text{H}}(x)\phi_{\text{k}}^{[\text{L}]}(x)$ through the asymptotic behavior of the susceptibility of the interacting system:

$$\chi(x, x'; \omega) \xrightarrow{x \rightarrow \infty} \frac{\sqrt{\rho(x)}}{ik} \phi_{\text{H}}(x') \phi_{\text{k}}^{[\text{L}]}(x') e^{ikx} \quad (\text{B.26})$$

$$\xrightarrow{x > x' \rightarrow \infty} \frac{\sqrt{\rho(x)\rho(x')}}{ik} e^{ikx} [e^{-ikx'} + r e^{ikx'}] \quad (\text{B.27})$$

Inserting Eqs.(B.24)-(B.27) into the Dyson-like Eq.(2.1) all the x and x' dependence drops away, resulting in:

$$r = r_s + \frac{1}{ik} \int_{-\infty}^{\infty} dx \phi_{s_{\text{H}}}(x) \phi_{s_{\text{k}}}^{[\text{L}]}(x) f_{\text{HXC}}(\epsilon + I) \phi_{\text{H}}(x) \phi_{\text{k}}^{[\text{L}]}(x) \quad . \quad (\text{B.28})$$

Finally, approximate $\phi_{\text{H}}(x)\phi_{\text{k}}^{[\text{L}]}(x) \sim \phi_{s_{\text{H}}}\phi_{s_{\text{k}}}^{[\text{L}]}(x)$ inside the integral. This corresponds to iterating once the Dyson-like Eq.(2.1), as in the Born approximation. This leads to Eq.(2.18) for the reflection amplitudes. The only difference for the transmission amplitudes is that one of the scattering orbitals of the f_{HXC} matrix element must satisfy the [R]-boundary condition, as can be seen by repeating the previous analysis for $x \rightarrow \infty$, and $x' \rightarrow \infty$, rather than $x > x' \rightarrow \infty$.

Appendix C

One electron: Susceptibility from the Green function.

Derivation of Eq.(2.13)

Consider an electron in the ground state $\phi_0(x)$ of a 1d-potential $v_s(x)$. In the absence of external time-dependent perturbations, its evolution is given by $\phi_0(x)e^{-i\varepsilon_0 t}$, where ε_0 is the ground-state energy. But due to a time-dependent perturbation $\delta v(x, t)$, this changes by an amount determined by the Green function $g_s(x, x'; t - t')$:

$$\delta\phi_0(x, t)e^{-i\varepsilon_0 t} = \int dx' \int dt' \phi_0(x')e^{-i\varepsilon_0 t'} g(x, x'; t - t') \delta v(x', t') . \quad (\text{C.1})$$

Since for one electron $\rho(x, t) = |\phi_0(x, t)|^2$, and $\delta\rho(x, t) = \phi_0(x, t)\delta\phi_0^*(x, t) + \phi_0^*(x, t)\delta\phi_0(x, t)$, taking the Fourier transform and comparing the resulting expression for $\delta\rho(x, \omega)$ with the defining equation of $\chi_s(x, x'; \omega)$:

$$\delta\rho(x, \omega) = \int dx' \chi_s(x, x'; \omega) \delta v(x'; \omega) , \quad (\text{C.2})$$

we get

$$\chi(x, x'; \omega) = \sqrt{\rho(x)\rho(x')} [g_s(x, x'; \omega + \varepsilon_0) + g_s^*(x, x'; -\omega + \varepsilon_0)] . \quad (\text{C.3})$$

Eq.(2.13) follows after setting $\omega = \varepsilon + I$ and $\varepsilon_0 = -I$.

Alternatively, expand $g_s(x, x'; \varepsilon)$ as a sum over states:

$$g(x, x'; \varepsilon) \equiv \langle x | (\varepsilon - \hat{H} + i\delta)^{-1} | x' \rangle = \sum_j \frac{\phi_j(x)\phi_j^*(x')}{\varepsilon - \varepsilon_j + i\delta} , \quad (\text{C.4})$$

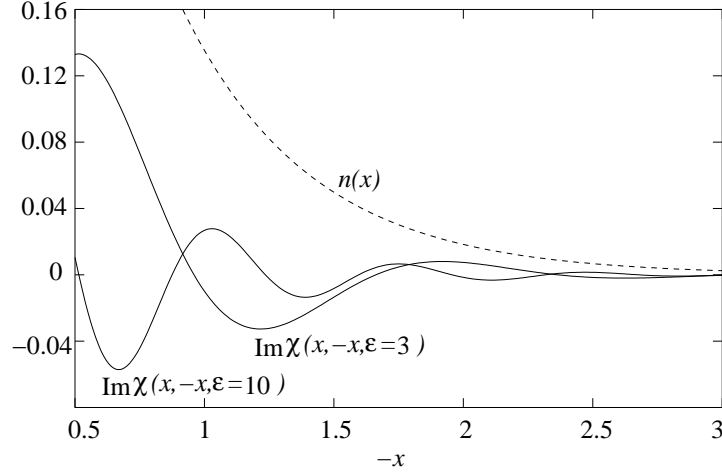


Figure C.1: Although $\chi_s(x, -x; \varepsilon)$ decays exponentially (because the density decays exponentially), it oscillates at large distances, and the amplitude of these oscillations yields the transmission coefficient. $Z = 1$ in this plot.

and compare with the 1-electron Lehman representation of $\chi_s(x, x'; \varepsilon + I)$ [27]:

$$\chi_s(x, x'; \varepsilon + I) = \sum_{j,k} (f_k - f_j) \frac{\phi_j(x) \phi_k^*(x) \phi_j^*(x') \phi_k(x')}{\varepsilon + I - (\varepsilon_j - \varepsilon_k) + i\delta} \quad (\text{C.5})$$

$$= \sqrt{\rho(x)\rho(x')} \left\{ \sum_{j \neq 0} \frac{\phi_j(x) \phi_j^*(x')}{\varepsilon - \varepsilon_j + i\delta} - \sum_{j \neq 0} \frac{\phi_j^*(x) \phi_j(x')}{\varepsilon + \varepsilon_j + 2I + i\delta} \right\} \quad (\text{C.6})$$

$$= \sqrt{\rho(x)\rho(x')} [g_s(x, x'; \varepsilon) + g_s^*(x, x'; -\varepsilon - 2I)] \quad (\text{C.7})$$

For the specific case of a negative delta-function potential of strength Z , the Green function $g_s(x, x'; \varepsilon)$ is known analytically, Eq.(2.16). We plot in Fig.(C.1) the imaginary part of χ_s at two different values of ε .

Appendix D

Hartree-exchange kernel for two contact-interacting electrons

For the spin-unpolarized ground-state of two contact-interacting electrons, as in the Hamiltonian of Eq.(2.21):

Hartree energy, potential, and kernel:

$$E_{\text{H}}[\rho] = \frac{\lambda}{2} \int dx \int dx' \rho(x) \rho(x') \delta(x - x') \quad (\text{D.1})$$

$$v_{\text{H}}^{\sigma}(x) = \frac{\delta E_{\text{H}}[\rho]}{\delta \rho_{\sigma}(x)} = \lambda \rho(x) \quad (\text{D.2})$$

$$f_{\text{H}}^{\sigma\sigma'}(x, x') = \frac{\delta v_{\text{H}}^{\sigma}(x)}{\delta \rho_{\sigma'}(x')} = \lambda \delta(x - x') \quad (\text{D.3})$$

Exchange energy, potential, and kernel:

$$E_{\text{X}}[\rho] = -\frac{\lambda}{4} \int dx \int dx' \rho(x) \rho(x') \delta(x - x') \quad (\text{D.4})$$

$$v_{\text{X}}^{\sigma}(x) = \frac{\delta E_{\text{X}}[\rho]}{\delta \rho_{\sigma}(x)} = -\lambda \rho_{\sigma}(x) \quad (\text{D.5})$$

$$f_{\text{X}}^{\sigma\sigma'}(x, x') = \frac{\delta v_{\text{X}}^{\sigma}(x)}{\delta \rho_{\sigma'}(x')} = -\lambda \delta_{\sigma\sigma'} \delta(x - x') \quad (\text{D.6})$$

Hartree-Exchange kernel:

$$f_{\text{HX}}^{\sigma\sigma'} = f_{\text{H}}^{\sigma\sigma'} + f_{\text{X}}^{\sigma\sigma'} = \lambda(1 - \delta_{\sigma\sigma'}) \delta(x - x') \quad (\text{D.7})$$

With the 1d-spin-decomposed version of Eq.(2.1),

$$\chi_{\sigma\sigma'}(x, x'; \omega) = \chi_{s\sigma\sigma'}(x, x'; \omega) + \sum_{\alpha, \beta} \int dy \int dz \chi_{s\sigma\alpha}(x, y) f_{\text{HX}}^{\alpha\beta}(y, z) \chi_{\beta\sigma'}(z, x') \quad (\text{D.8})$$

and the relation:

$$\chi_{s\sigma\sigma'}(x, x') = \delta_{\sigma\sigma'} \chi_{s\sigma\sigma}(x, x') \quad , \quad (\text{D.9})$$

insertion of the kernel (D.7) into Eq.(D.8) leads to:

$$\chi_{\uparrow\uparrow} = \chi_{s\uparrow\uparrow}(x, x') + \lambda \int dx'' \chi_{s\uparrow\uparrow}(x, x'') \chi_{\downarrow\uparrow}(x'', x') \quad (\text{D.10})$$

$$\chi_{\uparrow\downarrow}(x, x') = \lambda \int dx'' \chi_{s\uparrow\uparrow}(x, x'') \chi_{\downarrow\downarrow}(x'', x') \quad (\text{D.11})$$

Since the magnetic susceptibility \mathcal{M} is given by:

$$\mathcal{M} = \sum_{\sigma, \sigma'} (\sigma\sigma') \chi_{\sigma\sigma'} = 2\chi_{\uparrow\uparrow}(x, x') - 2\chi_{\uparrow\downarrow}(x, x') \quad (\text{D.12})$$

then:

$$\mathcal{M}(x, x'; \omega) = \chi_s(x, x'; \omega) - \frac{\lambda}{2} \int dx'' \chi_s(x, x''; \omega) \mathcal{M}(x'', x'; \omega) \quad , \quad (\text{D.13})$$

as in Eq.(2.30).

Appendix E

Numerical calculation of bound→free TDDFT matrix elements

E.1 Hartree-exchange

For two electrons, the Hartree-exchange kernel is given by $f_{\text{HX}} = \frac{1}{2} \frac{1}{|\mathbf{r}-\mathbf{r}'|}$. The Coulomb interaction can be expanded in Legendre polynomials as:

$$\frac{1}{|\mathbf{r}-\mathbf{r}'|} = \frac{1}{\sqrt{rr'}} \sum_{l=0}^{\infty} \left(\frac{r_{<}}{r_{>}} \right)^{l+\frac{1}{2}} P_l(\hat{\mathbf{r}} \cdot \hat{\mathbf{r}}') \quad , \quad (\text{E.1})$$

where $r_{<}$ and $r_{>}$ stand respectively for the lesser and greater of r and r' , the magnitudes of \mathbf{r} and \mathbf{r}' . For the spherically symmetric case at hand, we keep only the $l = 0$ term, yielding:

$$f_{\text{HX}} = \frac{1}{2r_{>}} \quad (\text{E.2})$$

Explicitly,

$$\langle\langle \mathbf{H}, \varepsilon | \hat{f}_{\text{HX}} | \mathbf{H}, \varepsilon \rangle\rangle = \frac{1}{2} \int d\mathbf{r} \int d\mathbf{r}' \frac{1}{(4\pi r r')^2} \phi_{\text{H}}(r) \phi_k(r) \frac{1}{r_{>}} \phi_{\text{H}}(r') \phi_k(r') \quad , \quad (\text{E.3})$$

with ϕ_{H} and ϕ_k being *radial* solutions of the $l = 0$ KS equations. Eq.(E.3) is rearranged to:

$$\langle\langle \mathbf{H}, \varepsilon | \hat{f}_{\text{HX}} | \mathbf{H}, \varepsilon \rangle\rangle = \frac{1}{2} \int_0^{\infty} dr (f_1(r) I_0(r) + f_0(r) [K - I_1(r)]) \quad , \quad (\text{E.4})$$

where:

$$\begin{aligned} f_0(r) &= \phi_{\text{H}}(r) \phi_k(r) \\ f_1(r) &= f_0(r)/r \end{aligned}$$

$$\begin{aligned}
I_0(r) &= \int_0^r f_0(r') dr' \\
I_1(r) &= \int_0^r f_1(r') dr' \\
K &= I_1(r \rightarrow \infty)
\end{aligned}$$

E.2 Correlation

The correlation kernel in the adiabatic local density approximation is given by:

$$f_c^{\text{ALDA}} = \frac{d^2 e_c^{\text{unif}}}{d\rho^2}(\rho_0) \delta^{(3)}(\mathbf{r} - \mathbf{r}') \quad , \quad (\text{E.5})$$

where e_c^{unif} is the correlation energy per particle of the uniform electron gas. With $\delta^{(3)}(\mathbf{r} - \mathbf{r}') = \delta(r - r')\delta(\theta - \theta')\delta(\phi - \phi')/(r^2 \sin \theta)$ the matrix elements of the kernel become:

$$\langle\langle \text{H}, \varepsilon | \hat{f}_c^{\text{ALDA}} | \text{H}, \varepsilon \rangle\rangle = \frac{1}{\pi} \int_0^\infty dr \frac{1}{r^2} |\phi_{\text{H}}(r)|^2 |\phi_k(r)|^2 \frac{d^2 e_c^{\text{unif}}}{d\rho(r)^2}(\rho_0) \quad . \quad (\text{E.6})$$

We calculated the second derivative of the Perdew-Wang parametrization of e_c^{unif} [84] as:

$$\frac{d^2 e_c^{\text{unif}}}{d\rho^2} = \frac{3^{-4/3}}{(4\pi)^{2/3}} n^{-5/3} G'' - \frac{2 \times 3^{-5/3}}{(4\pi)^{1/3}} n^{-4/3} G' \quad , \quad (\text{E.7})$$

where G' and G'' are the first and second derivatives with respect to $r_s = (3/4\pi\rho)^{1/3}$ of the G function of ref.[84]:

$$G' = -2A\alpha_1 q_2 - \frac{q_0 q_3}{q_1(1+q_1)} \quad , \quad (\text{E.8})$$

$$G'' = \frac{1}{q_1^2(1+1/q_1)} \left[2A(2\alpha_1 q_3 - q_0 q_4) + \frac{q_0 q_3^2}{q_1} \left(2 - \frac{1}{q_1(1+1/q_1)} \right) \right] \quad (\text{E.9})$$

with

$$q_0 = -2A(1 + \alpha_1 r_s) \quad (\text{E.10})$$

$$q_1 = 2A \left(\beta_1 \sqrt{r_s} + \beta_2 r_s + \beta_3 r_s^{3/2} + \beta_4 r_s^2 \right) \quad (\text{E.11})$$

$$q_2 = \ln \left(1 + q_1^{-1} \right) \quad (\text{E.12})$$

$$q_3 = A \left[\beta_1 / \sqrt{r_s} + 2\beta_2 + \sqrt{r_s} (3\beta_3 + 4\beta_4 \sqrt{r_s}) \right] \quad , \quad (\text{E.13})$$

and the constants A , α_1 , and $\beta_1 \dots \beta_4$ taken from ref.[84].

E.3 Note about the hybrid kernel employed

The BPG hybrid functional employed [49] sets to zero the parallel spin contribution to the correlation kernel, and to $f_C^{\uparrow\downarrow\text{ALDA}}$ the antiparallel contribution. The correction needed for *singlet* scattering in Section 2.3.1 is therefore given by the matrix elements of:

$$f_{\text{HXC}}^{\text{BPG}} = \frac{1}{2} \frac{1}{|\mathbf{r} - \mathbf{r}'|} + \frac{1}{2} f_C^{\uparrow\downarrow\text{ALDA}} \quad , \quad (\text{E.14})$$

whereas the corrections for *triplet* scattering are given by the matrix elements of the spin-flip kernel:

$$\Delta f_{\text{HXC}}^{\text{BPG}} = -f_{\text{HXC}}^{\text{BPG}} \quad (\text{E.15})$$

In the equations above, $f_C^{\uparrow\downarrow\text{ALDA}}$ is given by Eq(E.5) with the parameters of ref.[84] chosen for $\zeta = 0$ (unpolarized case).

Appendix F

High frequency behavior of optical response

Here we study the high frequency behavior of the dipole matrix elements $\langle np|\hat{r}|\varepsilon_{l=0}\rangle$ corresponding to transitions from $l = 1$ bound orbitals to $l = 0$ free orbitals, and then the elements $\langle ns|\hat{r}|\varepsilon_{l=1}\rangle$ corresponding to transitions from $l = 0$ bound orbitals to $l = 1$ free orbitals.

F.1 $p \rightarrow s$ transitions

For very high energies, the final states $|\varepsilon_{l=0}\rangle$ are plane waves with wavelength $k = \sqrt{2\varepsilon}$. We need to study the behavior of

$$\int_0^\infty dr \phi_{np}(r) r \sin kr \quad (\text{F.1})$$

as $k \rightarrow \infty$. Integrating by parts, one obtains

$$\int_0^\infty dr f(r) \sin kr = \frac{f(0)}{k} - \frac{f''(0)}{k^3} + \frac{f^{IV}(0)}{k^5} - \dots, \quad (\text{F.2})$$

where f^n stands for the n^{th} derivative with respect to r of the function $f(r) = r\phi_{np}(r)$. For coulombic ϕ_{np} 's, the second derivative $\phi_{np}''(0)$ is the first non-zero derivative at $r = 0$, so $f^{IV}(0) = 4\phi_{np}'''(0)$ is the first non-zero term in the expansion of Eq.(F.2), and the only term to be kept since $k \rightarrow \infty$. Taking into account the correct energy-normalization of the scattering state $\phi_k(r \rightarrow \infty) \rightarrow \sqrt{\frac{2}{\pi k}} \sin kr$, the result is:

$$\langle np|r|\varepsilon_{l=0}\rangle \xrightarrow{\infty} 4\sqrt{\frac{2}{\pi}}\phi_{np}'''(0)k^{-11/2} \quad (\text{F.3})$$

The cusp-condition

$$\phi_{np}'''(0) = -\frac{3}{2}Z\phi_{np}''(0), \quad (\text{F.4})$$

and substitution of $k = \varepsilon^2/2$ leads to:

$$\int_0^\infty dr \phi_{np}(r) r \phi_{\varepsilon, l=0} \xrightarrow{\varepsilon \rightarrow \infty} -\frac{3Z}{2^{5/4} \sqrt{\pi}} \phi_{np}''(r=0) \varepsilon^{-11/4} \quad (\text{F.5})$$

F.2 $s \rightarrow p$ transitions

$\langle ns | \hat{r} | \varepsilon_{l=1} \rangle$ Here we need to consider

$$\begin{aligned} \int_0^\infty dr \phi_{ns}(r) r F_1(0, kr) &= k \int_0^\infty dr \phi_{ns}(r) r^2 j_1(kr) \\ &= \frac{1}{k} I_1(k) - I_2(k) \quad , \end{aligned} \quad (\text{F.6})$$

where

$$\begin{aligned} I_1(k) &= \Im \int_0^\infty dr \phi_{ns}(r) e^{ikr} \\ &= \frac{\phi_{ns}(0)}{k} - \frac{\phi_{ns}''(0)}{k^3} + \frac{\phi_{ns}^{IV}(0)}{k^5} - \dots \quad , \end{aligned} \quad (\text{F.7})$$

and

$$\begin{aligned} I_2(k) &= \Re \int_0^\infty dr f(r) e^{ikr} \quad , \quad f(r) = r \phi_{ns}(r) \\ &= -\frac{f'(0)}{k^2} + \frac{f'''(0)}{k^4} - \frac{f^V(0)}{k^6} + \dots \\ &= \frac{3\phi_{ns}''(0)}{k^4} - \frac{5\phi_{ns}(0)}{k^6} + \dots \end{aligned} \quad (\text{F.8})$$

Taking into account the cusp condition $\phi_{ns}''(0) = -2Z\phi_{ns}'(0)$, and the normalization factor $\sqrt{2/\pi k}$, Eqs.(F.7) and (F.8), when inserted into Eq.(F.6), yield:

$$\int_0^\infty dr \phi_{ns}(r) r \phi_{\varepsilon, l=1}(r) \xrightarrow{\varepsilon \rightarrow \infty} \frac{8Z}{2^{7/4} \sqrt{\pi}} \phi_{ns}'(r=0) \varepsilon^{-9/4} \quad (\text{F.9})$$

References

- [1] A. Wright, K. Ziemelis, L. Sage, and K. Southwell, *Year of physics: a celebration*, Nature **433**, 213 (2005).
- [2] P.W. Anderson, *More is Different*, Science **177**, 393 (1972).
- [3] P. Hohenberg and W. Kohn, *Inhomogeneous electron gas*, Phys. Rev. **136**, B 864 (1964).
- [4] W. Kohn and L.J. Sham, *Self-consistent equations including exchange and correlation effects*, Phys. Rev. **140**, A 1133 (1965).
- [5] W. Kohn, *Nobel Lecture: Electronic structure of matter - wave functions and density functionals*, Rev. Mod. Phys. **71**, 1253 (1999).
- [6] K. Burke, *The ABC of DFT*, book in preparation (2006?).
- [7] R.M. Dreizler and E.K.U. Gross, *Density Functional Theory* (Springer-Verlag, Berlin, 1990).
- [8] J.P. Perdew and S. Kurth, *Density Functionals for Non-relativistic Coulomb Systems* in *Density functionals: Theory and applications*, ed. D. Joubert (Springer, Berlin, 1998).
- [9] M.H. Cohen and A. Wasserman, *New Developments in Density Functional Theory*, in *Proceedings of the International School of Physics "Enrico Fermi" Course CLV: The Physics of Complex Systems (New Advances and Perspectives)*, eds. F. Mallamace and H.E. Stanley, pp.253-295 (IOS Press, Amsterdam, 2004).
- [10] G. Hanel, B. Gstir, S. Denifl, P. Scheier, et.al., *Electron Attachment to Uracil: Effective Destruction at Subexcitation Energies* Phys. Rev. Lett. **90**, 188104 (2003).
- [11] M.A. Morrison, *The Physics of Low-energy Electron-Molecule Collisions: A Guide for the Perplexed and the Uninitiated*, Aust. J. Phys., **36**, 239 (1983); P.G.Burke, *Electron-Atom Scattering Theory and Calculations* Adv. Atom. Mol. Opt. Phys., **32**,39 (1994); C. Winstead and V. McKoy, *Electron Scattering by Small Molecules*, in *Advances in Chemical Physics*, ed. I. Prigogine and S.A. Rice, **XCVI**, 103 (1996).
- [12] A. Grandi, F.A. Gianturco, and N. Sanna, *H⁻ Desorption from Uracil via Metastable Electron Capture*, Phys. Rev. Lett. **93**, 048103 (2004).

- [13] e.g. *Electron-Atom Scattering Theory and Calculations*, P.G.Burke, Advances in Atomic, Molecular, and Optical Physics, **32**,39 (1994).
- [14] P.G.Burke, A.Hibbert, and D.W.Robb, *Electron Scattering by Complex Atoms*, J.Phys. B **4**, 153 (1971).
- [15] R.K.Nesbet, *Variational Methods in Electron-Atom Scattering Theory*, (Plenum Press, New York, 1980).
- [16] P.M.J.Sawey, K.A.Berrington, P.G.Burke, and A.E.Kingston, *Electron scattering by atomic hydrogen at intermediate energies. II. Differential elastic, 1s-2s and 1s-2p cross sections and 1s-2p electron-photon coincidence parameters*, J.Phys.B (At. Mol. Opt. Phys.) **24**, 2097 (1991).
- [17] A.G.Sunderland, C.J.Noble, V.M.Burke, and P.G.Burke, *A parallel R-matrix program PRMAT for electron-atom and electron-ion scattering calculations*, Comp.Phys.Comm. **145**, 311 (2002).
- [18] e.g. C.Lee, C.Winstead, and V.McKoy, *Collisions of low-energy electrons with CO₂*, J.Chem.Phys. **111**, 5056 (1999).
- [19] C. Ramsauer, *Über den Wirkungsquerschnitt der Kohlensäure-moleküle gegenüber langsamen Elektronen*, Ann. Phys. **83**, 1129 (1927).
- [20] T.N.Rescigno, D.A.Byrum, W.A.Isaacs, and C.W.McCurdy, *Theoretical studies of low-energy electron-CO₂ scattering: Total, elastic, and differential cross sections*, Phys.Rev. A **60**, 2186 (1999).
- [21] D.C. Langreth and M.J. Mehl, *Beyond the local-density approximation in calculations of ground-state electronic properties*, Phys. Rev. B **28**, 1809 (1983).
- [22] J.P. Perdew, K. Burke, and M. Ernzerhof, *Generalized Gradient Approximation Made Simple*, Phys. Rev. Lett. **77**, 3865 (1996); **78**, 1396 (1997) (E).
- [23] J. Tao, J.P. Perdew, V.N. Staroverov and G.E. Scuseria, *Climbing the Density Functional Ladder: Nonempirical Meta-Generalized Gradient Approximation Designed for Molecules and Solids*, Phys. Rev. Lett. **91**, 146401 (2003).
- [24] A. Görling, *Density-functional theory for excited states*, Phys. Rev. A **54**, 3912 (1996).
- [25] R. Gaudoin and K. Burke, *Lack of Hohenberg-Kohn theorem for excited states*, Phys. Rev. Lett. **93**, 173001 (2004).
- [26] E. Runge and E.K.U. Gross, *Density-functional theory for time-dependent systems*, Phys. Rev. Lett. **52**, 997 (1984).
- [27] K. Burke and E.K.U. Gross, *A guided tour of time-dependent density functional theory*, in *Density functionals: Theory and applications*, ed. D. Joubert (Springer, Berlin, 1998).

- [28] M.H. Cohen and A. Wasserman, *N-representability and stationarity in Time-dependent Density Functional Theory*, Phys. Rev. A, in press (2005) [cond-mat/0405532].
- [29] N.T. Maitra, K. Burke, H. Appel, E.K.U. Gross, and R. van Leeuwen, *Ten topical questions in time-dependent density functional theory*, in *Reviews in Modern Quantum Chemistry: A Celebration of the Contributions of R.G. Parr*, ed. K.D. Sen. (World Scientific,2001).
- [30] E.K.U. Gross and W. Kohn, *Local density-functional theory of frequency-dependent linear response*, Phys. Rev. Lett. **55**, 2850 (1985); **57**, 923 (1986) (E).
- [31] M. Petersilka, U.J. Gossmann, and E.K.U. Gross, *Excitation energies from time-dependent density-functional theory*, Phys. Rev. Lett. **76**, 1212 (1996).
- [32] H. Appel, E.K.U.Gross, and K. Burke, *Excitations in Time-Dependent Density-Functional Theory*, Phys. Rev. Lett. **90**, 043005 (2003).
- [33] A. Wasserman, N.T. Maitra, and K. Burke, *Continuum States from Time-dependent Density Functional Theory* J. Chem. Phys., in press (2005). [cond-mat/0503038].
- [34] J. Katriel and E.R. Davidson, *Asymptotic Behavior of Atomic and Molecular Wave Functions*, Proc. Natl. Acad. Sci. USA **77**, 4403 (1980).
- [35] M. Ernzerhof, K. Burke, and J.P. Perdew, *Long-Range Asymptotic Behavior of Ground-State Wavefunctions*, J. Chem. Phys. **105**, 2798 (1996).
- [36] N.T. Maitra, A. Wasserman, and K. Burke, *What is Time-dependent Density Functional Theory?: Successes and Challenges in Electron Correlations and Materials Properties 2*, ed. A. Gonis, N. Kioussis, and M. Ciftan (Kluwer Academic/Plenum Publishers, 2003).
- [37] A. Szabo and N.S. Ostlund, *Modern Quantum Chemistry: Introduction to Advanced Electronic Structure Theory*, McGraw-Hill, New York (1989).
- [38] D.J. Griffiths, *Introduction to Quantum Mechanics*, Sec.2.5., (Prentice Hall, 1995).
- [39] C.M. Rosenthal, *Solution of the Delta Function Model for Heliumlike Ions*, J. Chem. Phys. **55**, 2474 (1971).
- [40] B.H. Bransden and C.J. Joachain, *Physics of Atoms and Molecules* (Longman, New York, 1983).
- [41] E.H. Lieb, J.P. Solovej, and J. Yngvason, *Heavy atoms in the strong magnetic field of a neutron star*, Phys. Rev. Lett. **69**, 749 (1992).

- [42] R.J. Magyar, and K. Burke, *Density-functional theory in one dimension for contact-interacting fermions*, Phys. Rev. A **70**, 032508 (2004).
- [43] H. Friedrich, *Theoretical Atomic Physics*, Sec.3.1, (Springer, New York, 1991).
- [44] M. Petersilka and E.K.U. Gross, *Spin-multiplet energies from time-dependent density functional theory*, Int. J. Quant. Chem. Symp. **30**, 1393 (1996).
- [45] M.E. Casida, *Time-dependent density functional response theory of molecular systems: Theory, computational methods, and functionals*, in *Recent developments and applications in density functional theory*, ed. J.M. Seminario (Elsevier, Amsterdam, 1996).
- [46] A. I. Al-Sharif, R. Resta, C.J. Umrigar, *Evidence of physical reality in the Kohn-Sham potential: The case of atomic Ne*, Phys. Rev. A **57**, 2466 (1998).
- [47] M.J. Seaton, *The Quantum Defect Method*, Mon. Not. R. Astron. Soc. **118**, 504 (1958)
- [48] C. J. Umrigar and X. Gonze, *Accurate exchange-correlation potentials and total-energy components for the helium isoelectronic series*, Phys. Rev. A **50**, 3827 (1994).
- [49] K. Burke, M. Petersilka, and E.K.U. Gross, *A hybrid functional for the exchange-correlation kernel in time-dependent density functional theory*, in *Recent advances in density functional methods, vol. III*, ed. P. Fantucci and A. Bencini (World Scientific Press, 2000).
- [50] A.K. Bhatia, *Electron-He⁺ elastic scattering*, Phys. Rev. A **66**, 064702 (2002).
- [51] R.R. Lucchese and V. McKoy, *Application of the Schwinger variational principle to electron-ion scattering in the static-exchange approximation* Phys. Rev. A **21**, 112 (1980).
- [52] A. Gonis, *Green Functions for Ordered and Disordered Systems*, Studies in Mathematical Physics, Vol. 4, eds. E. van Groesen and E.M. de Jager, (Elsevier Science Publishers B.V., North-Holland, 1992).
- [53] B.Y. Tong, and L.J. Sham, *Application of a Self-Consistent Scheme Including Exchange and Correlation Effects to Atoms*, Phys. Rev. **144**, 1 (1966).
- [54] F. Della Salla and A. Görling, *The asymptotic region of the Kohn-Sham exchange potential in molecules*, J. Chem. Phys. **116**, 5374 (2002).
- [55] M. Grüning, O.V. Gritsenko, S.J.A. van Gisbergen, and E.J. Baerends, *On the required shape corrections to the local density and generalized gradient approximations to the Kohn-Sham potentials for molecular response calculations*

- of (hyper)polarizabilities and excitation energies, *J. Chem. Phys.* **116**, 9591 (2002).
- [56] R. van Leeuwen and E.J. Baerends, *Exchange-correlation potential with correct asymptotic behavior*, *Phys. Rev. A.* **49**, 2421 (1994).
- [57] M.E. Casida and D.R. Salahub, *Asymptotic correction approach to improving approximate exchange-correlation potentials: Time-dependent density-functional theory calculations of molecular excitation spectra*, *J. Chem. Phys.* **113**, 8918 (2000).
- [58] D.J. Tozer and N.C. Handy, *On the determination of excitation energies using density functional theory*, *Phys. Chem. Chem. Phys.* **2**, 2117 (2000).
- [59] T. Grabo, T. Kreibich, S. Kurth, and E.K.U. Gross, *Orbital functionals in density functional theory: the optimized effective potential method*, in *Strong Coulomb correlations in electronic structure: Beyond the local density approximation*, ed. V.I. Anisimov (Gordon and Breach, Tokyo, 1998).
- [60] S. Kümmel and J.P. Perdew, *Simple iterative construction of the optimized effective potential for orbital functionals, including exact exchange*, *Phys. Rev. Lett.* **90**, 043004 (2003).
- [61] K. Yabana and G.F. Bertsch, *Time-dependent local-density approximation in real time*, *Phys. Rev. B* **54**, 4484 (1996).
- [62] A. Rubio, J.A. Alonso, X. Blase, L.C. Balbás, and S. G. Louie, *Ab Initio Photoabsorption Spectra and Structures of Small Semiconductor and Metal Clusters*, *Phys. Rev. Lett.* **77**, 247 (1996).
- [63] I. Vasiliev, S. Ögüt, and J.R. Chelikowsky, *Ab Initio Excitation Spectra and Collective Electronic Response in Atoms and Clusters*, *Phys. Rev. Lett.* **82**, 1919 (1999).
- [64] I. Vasiliev, S. Ögüt, and J.R. Chelikowsky, *First-principles density-functional calculations for optical spectra of clusters and nanocrystals*, *Phys. Rev. B* **65**, 115416 (2002).
- [65] A. Zangwill and P. Soven, *Density-functional approach to local-field effects in finite systems: Photoabsorption in the rare gases*, *Phys. Rev. A* **21**, 1561 (1980).
- [66] G.D. Mahan and K.R. Subbaswamy, *Local Density Theory of Polarizability* (Plenum, New York, 1990)
- [67] A. Zangwill *A Time-Dependent Local Density Approximation of Atomic Photoionization*, in *Atomic Physics 8*, eds. I. Lindgren, A. Rosén, and A. Svanberg (Plenum, New York, 1983), p.347.

- [68] J.P. Perdew, *What do the Kohn-Sham orbitals mean? How do atoms dissociate?*, in *Density Functional Methods in Physics*, eds. R.M. Dreizler and J. da Providencia (Plenum, New York, 1985), p. 265.
- [69] E. Engel and R.M. Dreizler, *From explicit to implicit density functionals*, J. Comput. Chem. **20**, 31 (1999).
- [70] M. Petersilka, E.K.U. Gross, and K. Burke, *Excitation energies from time-dependent density functional theory using exact and approximate functionals*, Int. J. Quantum Chem. **80**, 534 (2000).
- [71] E.P. Wigner, *On the Behavior of Cross Sections Near Thresholds*, Phys. Rev. **73**, 1002 (1948).
- [72] M. Stener, P. Decleva, and A. Görling, *The role of exchange and correlation in time-dependent density-functional theory for photoionization*, J. Chem. Phys. **114**, 7816 (2001).
- [73] A. Kono and S. Hattori, *Accurate oscillator strengths for neutral helium*, Phys. Rev. A **29**, 2981 (1984).
- [74] J.A. R. Samson, Z.X. He, L. Yin, and A. Haddad, *Precision measurements of the absolute photoionization cross sections of He* J. Phys. B. **27**, 887 (1994).
- [75] W. Kohn, Y. Meir, and D.E. Makarov, *Van der Waals Energies in Density Functional Theory*, Phys. Rev. Lett. **80**, 4153 (1998).
- [76] A.J. Misquitta, B. Jeziorski, and K. Szalewicz, *Dispersion energy from Density-Functional Theory Description of Monomers*, A.J. Misquitta, B. Jeziorski, and K. Szalewicz, Phys. Rev. Lett. **91**, 033201, (2003).
- [77] A. Wasserman, N.T. Maitra, and K. Burke, *Accurate Rydberg Excitations from the Local Density Approximation*, Phys. Rev. Lett. **91**, 263001 (2003).
- [78] J.P. Perdew, *What do the Kohn-Sham Orbital Energies Mean? How do Atoms Dissociate?*, in *Density Functional Methods in Physics*, edited by R.M. Dreizler and J. da Providencia (Plenum, New York, 1985), p.265.
- [79] F. Ham, in *Solid State Physics*, Vol.1, edited by F. Seitz and D. Turnbull (Academic Press, 1955), p.127.
- [80] U. Fano, *Evolution of Quantum-defect Methods*, Comments Atom. Mol. Phys. **10**, 223 (1981).
- [81] L.J. Slater, *Confluent Hypergeometric Functions*, in *Handbook of Mathematical Functions*, ed. M. Abramowitz and I.A. Stegun, (Dover, New York, 1970), p.505.
- [82] J.H. Eberly, *Quantum Scattering Theory in One Dimension*, Am. J. Phys. **33**, 771, (1965).

- [83] V.E. Barlette, M.M. Leite, and S.K. Adhikari, *Integral equations of scattering in one dimension*, Am. J. Phys. **69**, 1010 (2001).
- [84] J. P. Perdew and Y. Wang, *Accurate and simple analytic representation of the electron-gas correlation energy*, Phys. Rev. B **45**, 13244 (1992).

Curriculum Vitae

Adam Wasserman

Work Address and telephone:

Department of Chemistry
Rutgers University
Piscataway, NJ 08854
(732) 445-7941
e-mail: awasser@rutchem.rutgers.edu

Home address and telephone:

303 N 3rd. Ave., Apt.A
Highland Park, NJ 08904
(732) 729-1842

Education

Rutgers University, New Brunswick, NJ
Ph.D., Chemistry, expected May 2005.

Universidad Nacional de Colombia
B.A., Chemistry, Feb.1993 - Aug.1999.

Publications

- A. Wasserman y V. Niño, *Efecto de la periodicidad del potencial de pares sobre el espectro de energía de las cuasipartículas en un superconductor*, Revista Colombiana de Física, **31** (2), 287 (1999).
- A. Wasserman y V. Niño, *Origen de la relación de autoconsistencia del parámetro de orden en superconductividad*, Revista Colombiana de Física, **32** (1), 109 (2000).
- N.T.Maitra, A. Wasserman, and K. Burke, *What is time-dependent density functional theory? Successes and Challenges*, in *Electron Correlations and Materials Properties 2*, eds. A. Gonis, N. Kioussis, and M. Ciftan, Kluwer Academic/Plenum Publishers, pp. 285-298 (2003).
- A. Wasserman, N.T. Maitra, and K. Burke, *Accurate Rydberg Excitations from the Local Density Approximation*, Phys. Rev. Lett. **91**, 263001 (2003).
- M.H. Cohen and A. Wasserman, *Revisiting N-continuous Density-Functional Theory: Chemical Reactivity and "Atoms in Molecules"*, Israel J. Chem. **43**, 219 (2003).

- M.H. Cohen and A. Wasserman, *New Developments in Density Functional Theory*, in *Proceedings of the International School of Physics “Enrico Fermi” Course CLV: The Physics of Complex Systems (New Advances and Perspectives)*, eds. F. Mallamace and H.E. Stanley, pp.253-295 (IOS Press, Amsterdam, 2004).
- A. Wasserman, N.T. Maitra, and K. Burke, *Continuum States from Time-dependent Density Functional Theory*, *J. Chem. Phys.*, accepted (2005) [cond-mat/0503038].
- M.H. Cohen and A. Wasserman, *N-representability and stationarity in Time-dependent Density Functional Theory*, *Phys. Rev. A*, accepted (2005) [cond-mat/0405532].

Personal Information

- Born in Jerusalem, Israel.
- Grew up in Paradise: Colombia.
- Hobby: piano.